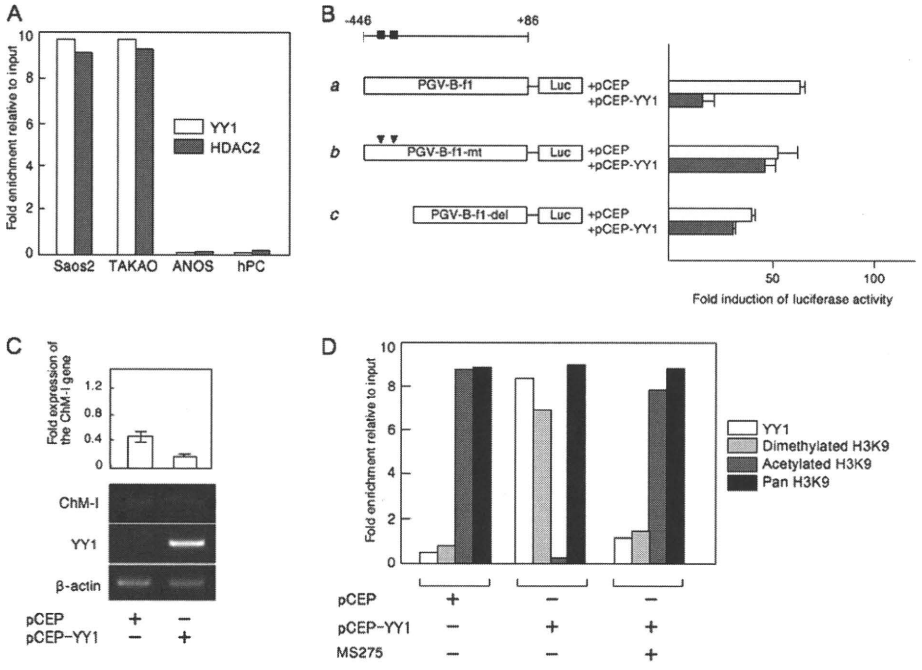

FIGURE 3. **YY1 bound to the regulatory region of *ChM-I* and decreased the promoter activity of *ChM-I*.** *A*, ChIP-qPCR assay for YY1 and HDAC2. *B*, luciferase reporter assay. *a*, DNA fragment encompassing −446 to +86 was cloned into a reporter vector containing the luciferase gene (*PGV-B-f1*). The *black box* indicates the location of the consensus sequence for the YY1-binding motif. *b*, PGV-B-f1-mt contains mutations in the YY1-binding motif (*arrowhead*), and PGV-B-f1-del lacked the YY1-binding motifs (*c*). Each reporter vector was co-transfected with empty vector (*pCEP*) or the YY1 expression vector (*pCEP-YY1*) into ANOS. The fold-increase was calculated based on empty vector activity. *C*, expression of endogenous *ChM-I* in hPCs transfected with the YY1 expression vector. The expression of *ChM-I* was semi-quantified taking the value for endogenous expression as 1.0 and is demonstrated at the *top*. *D*, ChIP-qPCR assay of hPCs transfected with the YY1 expression vector with or without MS275 treatment (1 μM for 24 h). Forced expression of YY1 in hPCs changed the modification of the H3 tail from acetylation to dimethylation.

that the core-promoter region was hypermethylated, which was similar to those that found in NHOSTs (Fig. 1*B*). In other tissues, the core-promoter region was hypomethylated. These results further suggested a mechanism other than DNA methylation to down-regulate the expression of *ChM-I*.

A search for factors regulating the chromatin structure revealed two tandem repeats (−344 to −347 and −342 to −346) of the binding motif of YY-1, which represses gene expression by recruiting HDAC to target regions (13, 14). As for factors with HAT activity, we focused on p300, which is known to relieve the transcriptional repression by YY1 (19). p300 also plays a role as a transcriptional adaptor recruiting transcription factors such as Sp3 (20). ChIP-qPCR assay showed that YY1 and HDAC2 bound to the core-promoter region in ChM-I-negative hMSCs, NHOSTs, and hPAs, whereas p300 and Sp3 bound in ChM-I-positive hPC (Fig. 2*C*). Consistent with the results obtained with primary-cultured cells, p300 and Sp3 bound to the core-promoter region in cells of cartilage, but not bone, fat or nerve tissue (Fig. 2*D*). On the other hand, the binding of YY1 and HDAC2 was observed in cells of bone, fat, and nerve, but not cartilage (Fig. 2*D*). ChIP-qPCR assay of the histone tail associated with the core-promoter region demonstrated that H3K9 was acetylated in cells of cartilage tissue, and dimethylated in those of bone, fat, and nerve tissues (Fig. 2*E*), which corresponded with the expression of *ChM-I* in each tissue. These results indicated that the expression of *ChM-I* correlated positively with the binding of p300 and negatively with that of YY1.

YY1 Binds to the Core Promoter Region and Inhibits Transcription—To further analyze the involvement of YY1 and p300 in the regulation of *ChM-I*, we used an osteosarcoma cell line, ANOS, as a ChM-I positive cell line, which we have previously investigated. The core-promoter region of the gene was hypomethylated in ANOS cells (2). As ChM-I-negative cell lines, two other osteosarcoma cell lines, Saos2 and TAKAO, were used, in which the core-promoter region was hypermethylated (2).

ChIP-qPCR assays showed that YY1and HDAC2 bound to the regulatory region of Saos2 and TAKAO cells, but not ANOS cells and hPCs (Fig. 3*A*). The binding of YY1 was further confirmed by an EMSA using an oligonucleotide (OND) (GR3) containing putative YY1-binding motifs (−342 to −347) (supplemental Fig. S2*A*). A shifted band was detected in the protein-OND complex from Saos2 cells, which disappeared on competition with unlabeled OND (supplemental Fig. S2*A*, *left panel*). The shifted band was detected also in the protein-OND complex from TAKAO cells, but not in ChM-I-positive cells (ANOS cells and hPCs) (supplemental Fig. S2*A*, *middle panel*). The shifted band was further shifted by the pretreatment with anti-YY1 antibody (supplemental Fig. S2*A*, *right panel*). These results indicated that YY1 bound to the core-promoter region of *ChM-I* in ChM-I-negative cells. To analyze the functional involvement of YY1, a reporter assay using the promoter fragment (−446 to +86) was performed (Fig. 3*B*), which contained the basal transcriptional activity of *ChM-I* (2). When the YY1 expression vector was co-transfected with the reporter plasmid, the promoter activity was significantly inhibited in ANOS cells (Fig. 3*B*, *a*). This inhibitory effect of YY1 was not observed when the reporter vector was replaced with one containing mutations in the YY1 motif (Fig. 3*B*, *b*) or lacking the motif (Fig. 3*B*, *c*). Forced expression of YY1 inhibited the expression of the endogenous *ChM-I* gene in hPCs (Fig. 3*C*), which was associated with the deacetylation and dimethylation of H3 (Fig. 3*D*). Co-treatment with MS275 inhibited the effect of forced expression of YY-1, rescuing the acetylation of H3K9 (Fig. 3*D*). These results suggested that YY1 inhibits the transcriptional activity of *ChM-I* by binding to a putative binding motif in the core-promoter region.

p300 Binds to the Core Promoter Region and Enhances Transcription—ChIP-qPCR assays showed that p300 as well as Sp3 bound to the core-promoter region of *ChM-I* in ANOS cells and hPCs, but not Saos2 and TAKAO cells (Fig. 4*A*). H3K9 associated with this region was acetylated in ANOS cells and

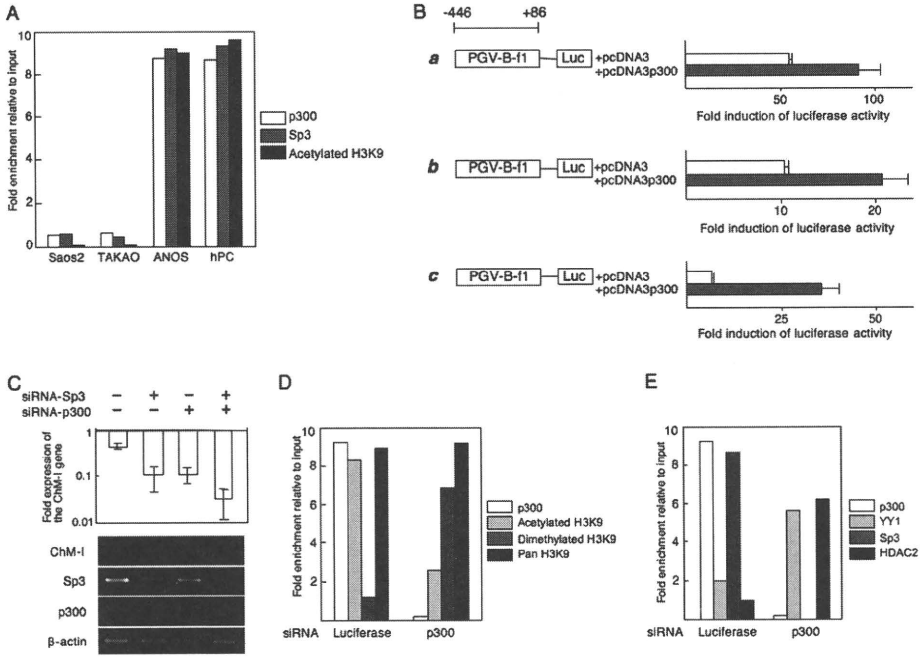

FIGURE 4. **p300 binds to the core promoter region and enhances transcription.** *A*, ChIP-qPCR assay of p300, Sp3 and acetylated H3. *B*, luciferase reporter assay. The reporter construct was described in the legend for Fig. 3*B*, and co-transfected with empty vector (pcDNA3) or the p300 expression vector (pcDNA3-p300) into ANOS (*a*), Saos2 (*b*), or TAKAO (*c*). The fold-increase was calculated based on empty vector activity. *C*, down-regulation of ChM-I gene expression by siRNA for Sp3 and/or p300. siRNAs for Sp3 and/or p300 were transfected into ANOS, and the expression of ChM-I, Sp3, and p300 was analyzed by RT-PCR. The expression of *ChM-I* was semi-quantified taking the value for endogenous expression as 1.0 and is demonstrated at the *top*. *D*, ChIP-qPCR assay for the modification of H3K9 (*D*) and for the binding of transcription regulators (*E*): cross-linked DNA-protein complexes were prepared from ANOS treated with or without siRNA for p300 and used for ChIP-qPCR assay.

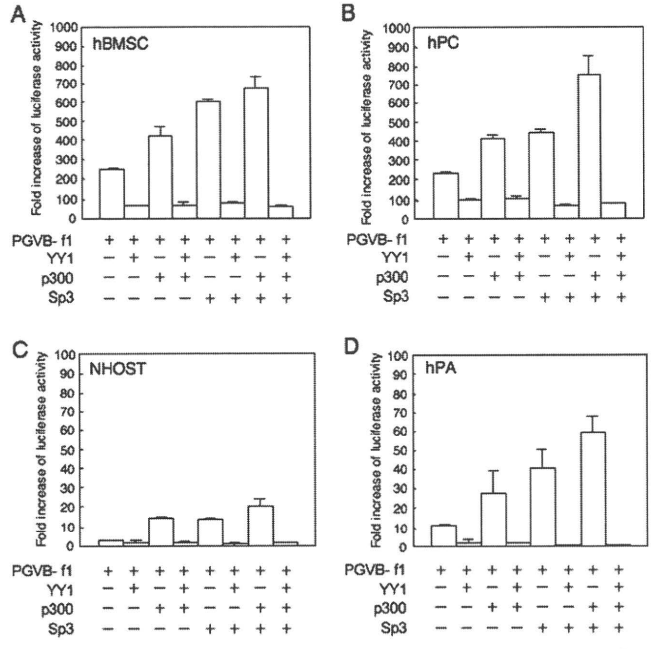

FIGURE 5. **Promoter activity of *ChM-I* was promoted by Sp3 and p300, but completely inhibited by YY1 in primary cultured cells.** The luciferase reporter vector containing the core-promoter fragment of the *ChM-I* gene (*PGV-B-f1*) was co-transfected with YY1, p300 and/or Sp3 expression vectors into hMSCs (*A*), hPCs (*B*), NHOSTs (*C*), and hPAs (*D*). The fold-increase was calculated based on empty vector activity.

hPCs, but not Saos2 or TAKAO cells (Fig. 4*A*). The binding of p300 was further confirmed by an EMSA using an OND (GR4)-containing putative p300 and Sp3-binding motifs (−56 to −48) (supplemental Fig. S2*B*). A shifted band was observed in extracts from ANOS cells, but not Saos2 or TAKAO cells (supplemental Fig. S2*B*, *middle panel*). The specificity of the band was confirmed by addition of a cold OND (supplemental Fig. S2*B*, *left panel*). The shifted band was supershifted when cell extracts were pretreated with anti-Sp3 antibody, and the same band disappeared when cell extracts were pretreated with anti-p300 antibody (supplemental Fig. S2*B*, *right panel*), suggesting that the protein-OND complex contained both Sp3 and p300. The functional involvement of p300 was analyzed with a promoter assay. Promoter activity was increased by co-transfection of the p300 expression vector in both ChM-I-positive (ANOS, Fig. 4*B*, *a*) and negative (Saos2, Fig. 4*B*, *b*; TAKAO, Fig. 4*B*, *c*) cells. Inhibition of p300 or Sp3 expression by the siRNA for each gene (siRNA-p300 and siRNA-Sp3) reduced the expression of *ChM-I* in PCs, while the two siRNAs combined had an additive effect (Fig. 4*C*). ChIP-qPCR assays showed that the siRNA for p300 changed H3K9 from an acetylated to dimethylated form (Fig. 4*D*). These results suggest that p300 positively regulates the transcriptional activity of *ChM-I* by inducing the acetylation of H3K9 associated with this region.

Involvement of YY1 and p300 in Primary Mesenchymal Cells—The effect of YY1 and p300 on promoter activity was further analyzed in primary-cultured mesenchymal cells (Fig. 5). Surprisingly, the transcriptional activity of the basal promoter fragment in hMSCs (Fig. 5*B*) was as strong as those in hPCs (Fig. 5*A*), although the expression of endogenous *ChM-I* was weak in hMSCs. In contrast, the basal activity level was low in NHOSTs and hPAs (Fig. 5, *C* and *D*). When the YY1 expression vector was co-transfected with the reporter vector, promoter activity was significantly inhibited in all strains (Fig. 5, *A–D*). Co-transfection with the p300 or Sp3 expression vector enhanced the activity, and simultaneous transfection of the two vectors increased it in an additive manner (Fig. 5, *A–D*). The enhancement of *ChM-I* expression by the p300 and/or Sp3 expression vectors was completely inhibited by the co-transfection of YY1 in all strains (Fig. 5, *A–D*). These results confirmed that YY1 and p300 are involved in the regulation of *ChM-I* transcription in mesenchymal cells, and that because this luciferase reporter system has no relationship with histone modifications, YY1

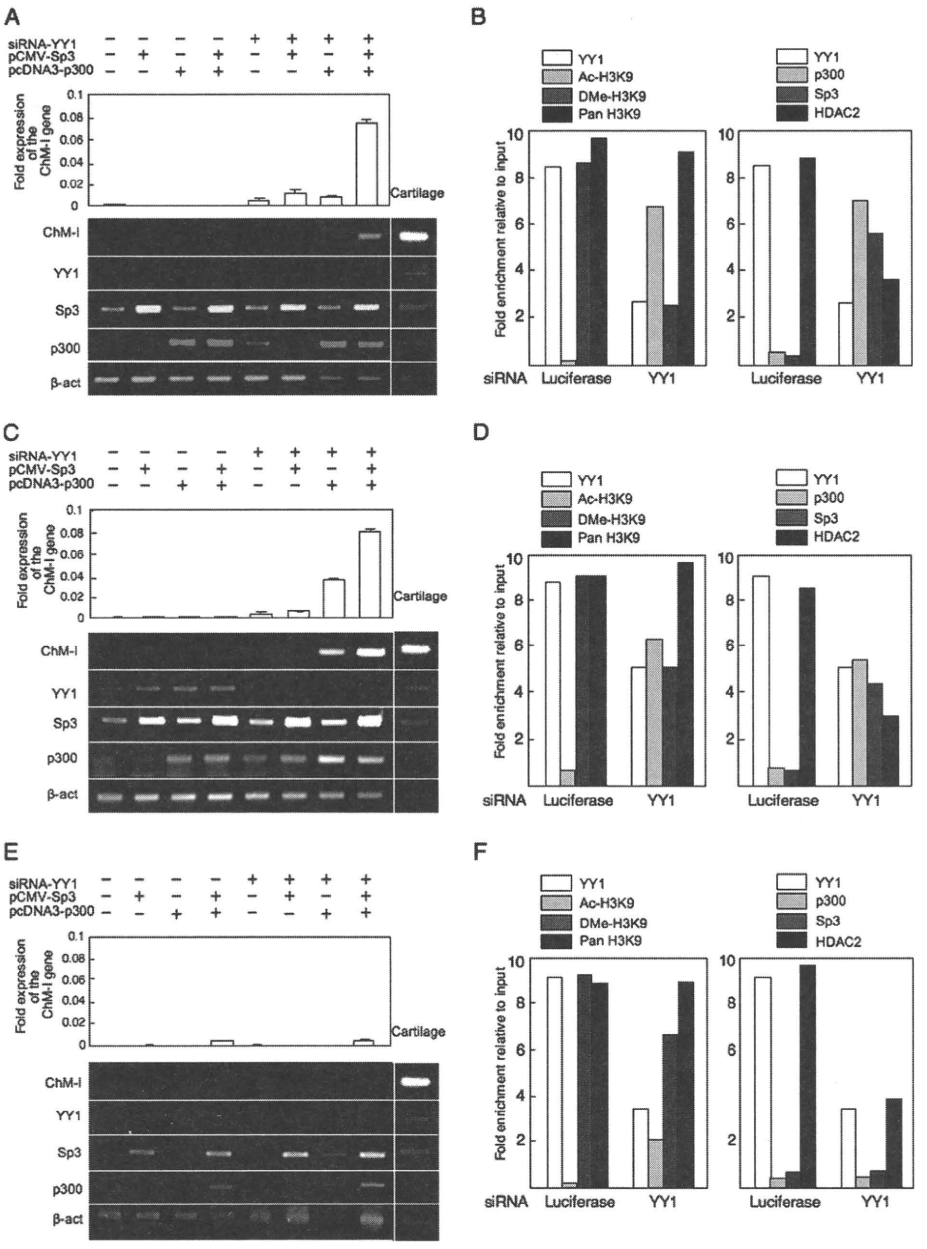

FIGURE 6. **Induction of *ChM-I* expression in ChM-I-negative primary cultured cells by modification of regulators.** *A–C*, primary-cultured cells were transfected with a combination of the siRNA for YY1, p300 expression vector, and Sp3 expression vector, and mRNA level of *ChM-1*, *YY1*, *p300*, and *Sp3* gene were analyzed by semi-quantitative RT-PCR (*lower panel*). The expression of the *ChM-I* was further analyzed by quantitative RT-PCR and digitalized (*upper panel*). *A*, hMSCs; *C*, hPAs; *E*, NHOSTs. ChIP-qPCR assay: *B*, hMSCs; *D*, hPAs; *F*, NHOSTs. Cross-linked DNA-protein complexes were prepared from primary cultured cells treated with or without siRNA for YY1 and used for ChIP-qPCR assay for the modificationf H3K9 (*left panels*) and for the binding of transcription regulators (*right panels*).

may directly inhibit the function of p300 or p300/Sp3 complex in addition to the modification of chromatin structure.

Cell-specific Effects of YY1 Inhibition on the Expression of ChM-I—Finally, the effect of YY1 expression on endogenous ChM-I expression was evaluated using siRNA for the gene (siRNA-YY1). In hMSCs (Fig. 6*A*), the inhibition of YY1 expression slightly induced the expression of *ChM-I* gene. The introduction of the p300 and/or Sp3 expression vectors had little effect on the expression of *ChM-I*, but significantly up-regulated it when combined with siRNA-YY1. Similar results were obtained in hPAs (Fig. 6*C*). In both cell types, siRNA-YY1 treatment induced the acetylation of H3K9 along with reductions in the dimetylation of H3K9 (Fig. 6, *B* and *D*, *left panels*). At the same time, siRNA-YY1 treatment dissociated HDAC2 and recruited p300 and Sp3 in the core-promoter region of *ChM-I* (Fig. 6, *B* and *D*, *right panels*). In NHOSTs (Fig. 6*E*), however, the combination the inhibition of YY1 and over-expression of p300 and Sp3 showed little effect for the induction of *ChM-I* expression. siRNA-YY1 treatment failed to induce the acetylation of H3K9 (Fig. 6*F*, *left panel*). Interestingly, although p300 was successfully recruited to the promoter region, no binding of Sp3 was observed in NHOSTs (Fig. 6*F*, *right panel*). These results suggested that Sp3 and p300 independently bind to the promoter region, and the binding of Sp3 was inhibited by the methylation of target DNA, but that of p300 was not. Therefore, the expression of a cartilage-specific gene, *ChM-I*, can be induced in some types of mesenchymal cells including MSCs by the modification of repressors (YY1) and activators (p300), but not in other cells, in which the expression is irreversibly inhibited by DNA methylation.

DISCUSSION

Numerous studies support the importance of epigenetic status for the regulation of differentiation, based on experiments involving chemical modifications of genome and the winding protein histone (21, 22). DNA methylation at CpG dinucleotides is a major epigenetic modification of the genome and associated with gene silencing (23). Because no intrinsic DNA-demethylating enzyme has been found, the inhibition by DNA methylation is tight under physiological conditions. Genomic DNA of embryonic stem (ES) cells is hypomethylated, and the total amount of methylated DNA increases with development (22, 24). Thus DNA methylation is a key mechanism to regulate and maintain the expression of cell type-specific genes. Unexpectedly, however, the methylation in the core-promoter region played a role in inhibiting the expression of *ChM-I* only

in particular types of mesenchymal cells; cells in bone (mainly osteocytes and osteoblasts) and peripheral nerve (mainly Schwann cells and perineural cells) (Fig. 2*A*). The hypomethylated status in hMSCs is reasonable considering the potential of these cells to differentiate. However, the core-promoter in terminally differentiated cells of a remote cell-lineage such as white blood cells was free from methylation and thus in a reversible state for gene expression (Fig. 2*A*). At present, we have no data to explain why some types of cells use DNA methylation to inhibit the expression of *ChM-I* and others do not. Cells of chondrogenic and osteogenic lineages are closely related, and may share a considerable proportion of transcriptional machinery. Therefore DNA methylation might be required to inhibit the expression of genes specific to chondro- or osteogenic lineages. The reporter assay gave almost identical results in hMSCs as in hPCs (Fig. 5, *A* and *B*), indicating that transcriptional machinery n hMSC to be ready to induce the expression of *ChM-I*, although there is no endogenous expression of the gene. This result strongly suggested that epigenetic machinery regulated the lineage-specific gene expression in stem cells.

The epigenetic status of each cell had been considered static, but recent a study demonstrated a dynamic nature to these modifications (25). We and others gave examples in which modification of the histone code induced a change of DNA methylation (3, 26). Notably, the modification of H3K9 strongly correlated with DNA methylation; dimethylated H3K9 correlated with hypomethylation and deacetylated H3K9 correlated with hypermethylation (9, 27). The recent discovery that the forced expression of transcription factors can reverse the epigenetic status of differentiated to that of ES cells is an extreme example of the dynamic nature of epigenetic status (28, 29). We showed that the expression of *ChM-I* was down-regulated by histone modifications in stem cells and some types of differentiated cells. The epigenetic status is induced and maintained by a number of intrinsic histone modifiers (30). In this study, we found that YY1 and p300 are main modifiers of histone associated with the core-promoter region of the ChM-I gene. YY1 is a DNA-binding zinc finger transcription factor, which has dual functions as an activator and a repressor (14). YY1 inhibits the transcription of target genes by competing for DNA-binding sites with activators, binding directly to activators, or recruiting co-repressors (14). One of these co-repressors is HDAC2, which was first identified as a binding partner of YY1 (13, 14). Previously, we demonstrated that HDAC2 bound to a histone tail associated with the core-promoter region of *ChM-I* in ChM-I-negative cells (3). In the present study, we showed that forced expression of YY1 deacetylated H3 associated with the core-promoter region in *ChM-I* (Fig. 3*E*), whereas HDAC2 was dissociated by the inhibition of YY1, causing acetylation of H3 (Fig. 6, *B*, *D*, and *F*). These results indicated that YY1 repressed the expression of *ChM-I* by recruiting HDAC2 to induce deacetylation of H3. Another repressive mechanism is the direct binding of p300, a binding partner of YY1 (14). p300 acts as an activator for target gene expression through intrinsic HAT activity (11, 12). Inhibition of p300 by siRNA resulted in the deacetylation of H3 and the repression of *ChM-I* expression (Fig. 5*C*), indicating the role of p300 as HAT for *ChM-I* expression. p300 also acts as a transcriptional co-activator for Sp3, not Sp1 (19), which is the main transcription factor of *ChM-I* (2). The exogenous expression of p300 enhanced the promoter activity in the reporter assay, suggesting the role of p300 as a co-activator. Inhibition of the promoter activity by the YY1 expression vector in the reporter assay indicated that YY1 acted as a direct repressor for p300 in addition to acting as a recruiter of HDAC (Fig. 6, *A*, *C*, and *E*). These results suggested that YY1 and p300 are involved in the regulation of *ChM-I* expression through the modification of histones and also the regulation of each others function.

It remains unclear how the repression of YY1 is relieved in chondrogenic cells. One possible mechanism is a post-translational modification of the YY1 protein. YY1 is glycosylated by *O*-linked *N*-acetylglucosaminylation, and glycosylated YY1 fails to bind to DNA (31). *O*-linked glucosamine is expressed in cartilage tissue (32). Such tissue-specific modifications may determine the expression of tissue-specific genes. It is also likely that tissue-specific chromatin-remodeling factors other than YY1 and p300 are involved in the regulation. Analyzing these issues may help to elucidate how the direction of differentiation is determined in stem cells.

Acknowledgments—We thank Dr. M. Nakanishi for providing MS-275 and helpful suggestions, Dr. K. Miyazono for the p300 expression vector, and Dr. E. Seto for the YY1 expression vector.

REFERENCES

1. Hiraki, Y., Tanaka, H., Inoue, H., Kondo, J., Kamizono, A., and Suzuki, F. (1991) *Biochem. Biophys. Res. Commun.* **175,** 971–977
2. Aoyama, T., Okamoto, T., Nagayama, S., Nishijo, K., Ishibe, T., Yasura, K., Nakayama, T., Nakamura, T., and Toguchida, J. (2004) *J. Biol. Chem.* **279,** 28789–28797
3. Aoyama, T., Okamoto, T., Kohno, Y., Fukiage, K., Otsuka, S., Furu, M., Ito, K., Jin, Y., Nagayama, S., Nakayama, T., Nakamura, T., and Toguchida, J. (2008) *Biochem. Biophys. Res. Commun.* **365,** 124–130
4. Noer, A., Sorensen, A. L., Boquest, A. C., and Collas, P. (2006) *Mol. Biol. Cell.* **17,** 3543–3556
5. Caplan, A. I. (1991) *J. Orthop. Res.* **9,** 641–650
6. Pittenger, M. F., Mackay, A. M., Beck, S. C., Jaiswal, R. K., Douglas, R., Mosca, J. D., Moorman, M. A., Simonetti, D. W., Craig, S., and Marshak, D. R. (1999) *Science* **284,** 143–147
7. Grunstein, M. (1997) *Nature* **389,** 349–352
8. Zhao, W., Soejima, H., Higashimoto, K., Nakagawachi, T., Urano, T., Kudo, S., Matsukura, S., Matsuo, S., Joh, K., and Mukai, T. (2005) *J. Biochem.* **137,** 431–440
9. Kondo, Y., Shen, L., and Issa, J. P. (2003) *Mol. Cell. Biol.* **23,** 206–215
10. Gan, Q., Yoshida, T., McDonald, O. G., and Owens, G. K. (2007) *Stem Cells* **25,** 2–9
11. Ogryzko, V. V., Schiltz, R. L., Russanova, V., Howard, B. H., and Nakatani, Y. (1996) *Cell* **87,** 953–959
12. Bannister, A. J., and Kouzarides, T. (1996) *Nature* **384,** 641–643
13. Yang, W. M., Yao, Y. L., Sun, J. M., Davie, J. R., and Seto, E. (1997) *J. Biol. Chem.* **272,** 28001–28007
14. Gordon, S., Akopyan, G., Garban, H., and Bonavida, B. (2006) *Oncogene* **25,** 1125–1142
15. Aoyama, T., Liang, B., Okamoto, T., Matsusaki, T., Nishijo, K., Ishibe, T., Yasura, K., Nagayama, S., Nakayama, T., Nakamura, T., and Toguchida, J. (2005) *J. Bone. Miner. Res.* **20,** 377–389
16. Shibata, K. R., Aoyama, T., Shima, Y., Fukiage, K., Otsuka, S., Furu, M., Kohno, Y., Ito, K., Fujibayashi, S., Neo, M., Nakayama, T., Nakamura, T., and Toguchida, J. (2007) *Stem Cells.* **25,** 2371–2382

17. Suske, G. (1999) *Gene* **238,** 291–300
18. Livak, K. J., and Schmittgen, T. D. (2001) *Methods* **25,** 402–408
19. Lee, J. S., Galvin, K. M., See, R. H., Eckner, R., Livingston, D., Moran, E., and Shi, Y. (1995) *Genes Dev.* **9,** 1188–1198
20. Kishikawa, S., Murata, T., Kimura, H., Shiota, K., and Yokoyama, K. K. (2002) *Eur. J. Biochem.* **269,** 2961–2970
21. Spivakov, M., and Fisher, A. G. (2007) *Nat. Rev. Genet.* **8,** 263–271
22. Bernstein, B. E., Meissner, A., and Lander, E. S. (2007) *Cell* **128,** 669–681
23. Esteller, M. (2007) *Nat. Rev. Genet.* **8,** 286–298
24. Reik, W., Dean, W., and Walter, J. (2001) *Science* **293,** 1089–1093
25. Klose, R. J., and Zhang, Y. (2007) *Nat. Rev. Mol. Cell Biol.* **8,** 307–318
26. Nakao, M. (2001) *Gene* **278,** 25–31
27. Rougeulle, C., Chaumeil, J., Sarma, K., Allis, C. D., Reinberg, D., Avner, P., and Heard, E. (2004) *Mol. Cell. Biol.* **24,** 5475–5484
28. Takahashi, K., Tanabe, K., Ohnuki, M., Narita, M., Ichisaka, T., Tomoda, K., and Yamanaka, S. (2007) *Cell* **131,** 861–872
29. Okita, K., Ichisaka, T., and Yamanaka, S. (2007) *Nature* **448,** 313–317
30. Pasini, D., Bracken, A. P., Agger, K., Christensen, J., Hansen, K., Cloos, P. A., and Helin, K. (2008) *Cold Spring Harb. Symp. Quant. Biol.***73,** 253–263
31. Hiromura, M., Choi, C. H., Sabourin, N. A., Jones, H., Bachvarov, D., and Usheva, A. (2003) *J. Biol. Chem.* **278,** 14046–14052
32. Thonar, E. J., Lohmander, L. S., Kimura, J. H., Fellini, S. A., Yanagishita, M., and Hascall, V. C. (1983) *J. Biol. Chem.* **258,** 11564–11570

Neurobiology of Disease

Induced Loss of ADAR2 Engenders Slow Death of Motor Neurons from Q/R Site-Unedited GluR2

Takuto Hideyama,[1,2] Takenari Yamashita,[1,2] Takeshi Suzuki,[3] Shoji Tsuji,[2] Miyoko Higuchi,[5] Peter H. Seeburg,[5] Ryosuke Takahashi,[6] Hidemi Misawa,[4] and Shin Kwak[1,2]

[1]Core Research for Evolutional Science and Technology, Japan Science and Technology Agency and [2]Department of Neurology, Graduate School of Medicine, University of Tokyo, Bunkyo-ku, Tokyo 113-8655, Japan, [3]Division of Basic Biological Sciences and [4]Department of Pharmacology, Faculty of Pharmacy, Keio University, Minato-ku, Tokyo 105-8512, Japan, [5]Department of Molecular Neuroscience, Max Planck Institute of Medical Research, 69120 Heidelberg, Germany, and [6]Department of Neurology, Graduate School of Medicine, University of Kyoto, Sakyo-ku, Kyoto 606-8507, Japan

GluR2 is a subunit of the AMPA receptor, and the adenosine for the Q/R site of its pre-mRNA is converted to inosine (A-to-I conversion) by the enzyme called adenosine deaminase acting on RNA 2 (ADAR2). Failure of A-to-I conversion at this site affects multiple AMPA receptor properties, including the Ca^{2+} permeability of the receptor-coupled ion channel, thereby inducing fatal epilepsy in mice (Brusa et al., 1995; Feldmeyer et al., 1999). In addition, inefficient GluR2 Q/R site editing is a disease-specific molecular dysfunction found in the motor neurons of sporadic amyotrophic lateral sclerosis (ALS) patients (Kawahara et al., 2004). Here, we generated genetically modified mice (designated as AR2) in which the ADAR2 gene was conditionally targeted in motor neurons using the Cre/loxP system. These AR2 mice showed a decline in motor function commensurate with the slow death of ADAR2-deficient motor neurons in the spinal cord and cranial motor nerve nuclei. Notably, neurons in nuclei of oculomotor nerves, which often escape degeneration in ALS, were not decreased in number despite a significant decrease in GluR2 Q/R site editing. All cellular and phenotypic changes in AR2 mice were prevented when the mice carried endogenous GluR2 alleles engineered to express edited GluR2 without ADAR2 activity (Higuchi et al., 2000). Thus, loss of ADAR2 activity causes AMPA receptor-mediated death of motor neurons.

Introduction

GluR2 (also known as GluR-B or GluA2) is a subunit of the AMPA receptor. The adenosine within the glutamine codon for the Q/R site of its pre-mRNA is converted to inosine (A-to-I conversion) (Yang et al., 1995) by adenosine deaminase acting on RNA 2 (ADAR2) (Melcher et al., 1996). Because inosine is read as guanosine during translation, the genomic glutamine codon (Q: CAG) is converted to a codon for arginine (R: CIG) at the Q/R site of GluR2 in virtually all neurons in the mammalian brain (Seeburg, 2002). Conversion of Q to R at the Q/R site of GluR2 affects multiple AMPA receptor properties, including the Ca^{2+} permeability of the receptor-coupled ion channel, receptor trafficking, and assembly of receptor subunits (Sommer et al., 1991; Burnashev et al., 1992; Greger et al., 2002, 2003). Genetically modified mice in which the Q/R site of GluR2 remains unedited displayed fatal status epilepticus at early postnatal stages with exaggerated excitation of neurons (Brusa et al., 1995; Feldmeyer et al., 1999). Systemic ADAR2-null mice exhibit a similar phenotype, which was attributed to the absence of GluR2 Q/R site RNA editing (Higuchi et al., 2000). These findings indicate that the A-to-I conversion of the GluR2 Q/R site by ADAR2 is crucial for survival in mice. However, it has not been demonstrated whether neuronal death occurs in mice lacking GluR2 Q/R site editing or in those lacking ADAR2.

Amyotrophic lateral sclerosis (ALS) is the most common adult-onset motor neuron disease. Patients with sporadic ALS account for >90% of all cases, and the majority of them do not carry mutations in the causative genes of familial ALS that have been identified thus far (Schymick et al., 2007; Beleza-Meireles and Al-Chalabi, 2009). There is strong evidence indicating that AMPA receptor-mediated excitotoxic mechanism plays a pathogenic role in ALS and SOD1-associated familial ALS model animals (Rothstein et al., 1992; Carriedo et al., 1996; Van Damme et al., 2005). Recently, we demonstrated that a significant proportion of GluR2 mRNA was unedited at the Q/R site in spinal motor neurons of postmortem patients with sporadic ALS. This is in marked contrast to the fact that all GluR2 mRNA was edited in the motor neurons of control subjects (Takuma et al., 1999; Kawahara et al., 2004) and of patients with motor neuron diseases other than sporadic ALS (Kawahara et al., 2006), as well as in dying neurons in other neurodegenerative diseases, including Purkinje cells of patients with spinocerebellar degeneration (Paschen et al., 1994; Akbarian et al., 1995; Kawahara et al., 2004; Suzuki et al., 2003). The disease specificity of inefficient GluR2 Q/R site editing implies the pathogenic relevance of ADAR2 insufficiency in the death of motor neurons in sporadic ALS but

Received April 20, 2010; revised July 2, 2010; accepted July 13, 2010.

This study was supported in part by Ministry of Education, Culture, Sports, Science, and Technology of Japan Grants-in-Aid for Scientific Research 17390251, 19390235, and 20023008 (S.K.), Ministry of Health, Labor, and Welfare of Japan Grant H18-Kokoro-017 (S.K.), and Amyotrophic Lateral Sclerosis Association Grant 875 (P.H.S.). We thank Dr. R. B. Emeson at Vanderbilt University (Nashville, TN) for antibodies to ADAR2 and D. Kimura, K. Awabayashi, Dr. J. Shimizu, Dr. M. Fukaya, and T. Kakinoki for technical assistance.

Correspondence should be addressed to Dr. Shin Kwak, Department of Neurology, Graduate School of Medicine, University of Tokyo, 7-3-1 Hongo, Bunkyo-ku, Tokyo 113-8655, Japan. E-mail: kwak-tky@umin.ac.jp.

DOI:10.1523/JNEUROSCI.2021-10.2010

 0270-6474/10/3011917-09$15.00/0

leaves open the possibility that other genes whose products remain unedited by ADAR2 insufficiency might contribute to the demise of motor neurons.

We therefore generated a conditional ADAR2 knock-out mouse strain (designated here as AR2), using the Cre/loxP recombination system, and demonstrated that the loss of ADAR2 activity induces the slow death of motor neurons also in the mouse. Importantly, all motor neuron death in AR2 mice could be prevented by substituting the wild-type GluR2 alleles for alleles point mutated to express Q/R site-edited GluR2 in the absence of ADAR2. Our genetic studies in the mouse clearly demonstrate that the underediting of the GluR2 Q/R site specifically induces death of motor neurons with reduced ADAR2 activity.

Materials and Methods

All studies were performed in accordance with the Declaration of Helsinki, the Guideline of Animal Studies of the University of Tokyo, and National Institutes of Health. The committee of animal handling of the University of Tokyo also approved the experimental procedures used.

ADAR2^{flox} *allele and conditional ADAR2 knock-out mice.* DNA for the targeted region was obtained from a mouse strain 129/SvEv genomic library (supplemental Table S1, available at www.jneurosci.org as supplemental material). A LoxP site was inserted into intron 6 and another LoxP site was inserted into intron 9 of the mouse *ADAR2* gene (*adarb1*), along with a selection cassette containing a neomycin resistance gene (Neo) flanked by flippase recognition target (FRT) sites (Fig. 1*A*). Exons 7–9 encode the majority of the adenosine deaminase motif. Chimeric mice were generated by injection of a targeted embryonic stem cell clone into C57BL/6-derived blastocysts. *ADAR2*$^{flox/+}$ intercrosses produced *ADAR2*$^{flox/flox}$ mice at apparent Mendelian frequencies, and *ADAR2*$^{flox/flox}$ homozygous mice were phenotypically normal. Determination of the *ADAR2*^{flox} allele was conducted by genomic PCR (Fig. 1*B*). Then, to knock-out ADAR2 activity selectively in motor neurons, we crossed *ADAR2*$^{flox/flox}$ mice with VAChT–Cre.Fast mice to obtain AR2 mice.

AR2 mice. Intercrosses of *ADAR2*$^{flox/+}$/VAChT–Cre.Fast mice produced *ADAR2*$^{flox/flox}$/VAChT–Cre.Fast (AR2) mice, either heterozygous or homozygous for the Cre transgene, which directs restricted Cre expression under the control of the vesicular acetylcholine transporter gene promoter in a subset of cholinergic neurons, including the spinal motor neurons (Misawa et al., 2003). Cre expression levels were found not to differ in mice heterozygous or homozygous for the VAChT–Cre.Fast transgene (Misawa et al., 2003). The same intercrosses also produced, as littermates of AR2, *ADAR2*$^{flox/flox}$ (Ctl1) and *ADAR2*$^{+/+}$/VAChT–Cre-.Fast mice (Ctl2), which were used as controls. Both genders of AR2 and control mice were used, but littermates heterozygous for the floxed ADAR2 allele were not used in this study. All genotyping was performed by PCR on DNA from tail biopsies. PCR primers and amplicon sizes for the different alleles are listed in supplemental Table S1 (available at www.jneurosci.org as supplemental material).

AR2/GluR-B$^{R/R}$ *mice.* AR2/GluR-$B^{R/R}$ mice were generated by intercrossing ADAR2$^{flox/+}$/VAChT–Cre.Fast/GluR-$B^{R/+}$mice, which had been produced by crossbreeding AR2 mice with GluR-$B^{R/R}$ mice. The AR2/GluR-$B^{R/R}$ mice used by us were either heterozygous or homozygous for the Cre transgene (Misawa et al., 2003) and homozygous for the floxed ADAR2 and the GluR-B(R) allele. The desired genotype was found approximately once in every 20 offspring. Other genotypes produced by the intercrosses were not used in this study. All genotyping for the ADAR2 and GluR2 (GluR-B) alleles as well as for the Cre transgene was by PCR on DNA extracted from tail biopsies. PCR primers and amplicon sizes for the different alleles are listed in supplemental Table S1 (available at www.jneurosci.org as supplemental material).

Genomic PCR and reverse transcription-PCR. Genomic DNA was extracted from mouse tails using the High Pure PCR Template Preparation kit (Roche). Total RNA was isolated from brain and spinal cord tissue, and first-strand cDNA was synthesized and then treated with DNase I (Invitrogen) as described previously (Kawahara et al., 2003b). Primer pairs and the conditions used for PCR are presented in supplemental Table S1 (available at www.jneurosci.org as supplemental material). Positions of primer pairs used for genomic ADAR2 PCR (Fig. 1*A*, F1/R1) and ADAR2 reverse transcription (RT)-PCR (Fig. 1*C*, F2/R2) are indicated.

Analysis for editing efficiency at A-to-I sites. Editing efficiencies at the Q/R sites in GluR2 mRNAs were calculated by quantitative analyses of the digests of RT-PCR products with BbvI as described previously (Takuma et al., 1999; Kawahara et al., 2003a, 2004). In brief, 2 μl of cDNA were subjected to first PCR in duplicate in a reaction mixture of 50 μl containing 200 mM each primer, 1 mM dNTP Mix (Eppendorf), 5 μl of 10× PCR buffer, and 1 μl of Advantage 2 Polymerase mix (Clontech). The PCR amplification began with a 1 min denaturation step at 95°C, followed by 40 cycles of denaturation at 95°C for 10 s, annealing at 60°C for 30 s, and extension at 68°C for 40 s. Nested PCR was conducted on 2 μl of the first PCR product under the same conditions with the exception of the annealing temperature (58°C). Primer pairs used for each PCR were listed in supplemental Table S1 (available at www.jneurosci.org as supplemental material). After gel purification using the Zymoclean Gel DNA Recovery kit according to the protocol of the manufacturer (Zymo Research), an aliquot (0.5 mg) was incubated with BbvI (New England Biolabs) at 37°C for 12 h. The PCR products originating from Q/R site-edited GluR2 mRNA had one intrinsic restriction enzyme recognition site, whereas those originating from unedited mRNA had an additional recognition site. Thus, restriction digestion of the PCR products originating from edited GluR2 mRNA should produce different numbers of fragments (two bands at 219 and 59 bp) from those originating from unedited GluR2 mRNA (three bands at 140, 79, and 59 bp). Because the 59 bp band would originate from both edited and unedited mRNA but the 219 bp band would originate from only edited mRNA, we quantified the molarity of the 219 and 59 bp bands using the 2100 Bioanalyzer (Agilent Technologies) and calculated the editing efficiency as the ratio of the former to the latter for each sample (supplemental Table S1, available at www.jneurosci.org as supplemental material).

With similar methods, we calculated the editing efficiencies at the Q/R sites in GluR5 and GluR6 mRNA and in GluR2 pre-mRNA, the R/G site in GluR2 mRNA, and the I/V site in Kv1.1 mRNA (Paschen et al., 1994; Takuma et al., 1999; Kawahara et al., 2003a, 2004; Nishimoto et al., 2008). The following restriction enzymes were used for restriction digestion of the respective A-to-I sites: BbvI for the Q/R sites, MfeI (New England Biolabs) for the I/V site, and MseI (New England Biolabs) for the R/G site. Primer pairs used for each PCR and sizes of restriction digests of PCR products were indicated in supplemental Table S1 (available at www.jneurosci.org as supplemental material).

Behavioral analyses. Using a mouse-specific rotarod (SN-445; Neuroscience Corp.), we determined the maximal time before falling at 10 rpm during a 180 s period; each run consisted of three trials. Grip strength was measured with a dynamometer (NS-TRM-M; Neuroscience Corp.). Measurements were conducted weekly by a researcher blind to genotype and age of the mice.

Isolation of single motor neurons and brain tissue. Single-cell isolation from frozen spinal cord tissue was performed with a laser microdissection system (Leica AS LMD; Leica Microsystems) as described previously (Kawahara et al., 2003b, 2004). All of the large motor neurons (diameter larger than 20 μm) in the anterior horn were dissected from 14-μm-thick cervical cord sections, and three neurons each were collected together into respective single test tubes containing 200 μl of TRIZOL Reagent. In addition, using the same method, nuclei of oculomotor nerve and of facial nerve were dissected from the brainstem sections of AR2 mice and control mice at 12 months of age. The positions of these cranial nerve nuclei were identified using the Paxinos and Franklin mouse brain atlas (Paxinos and Franklin, 2001). All samples were kept at −20°C until use.

Immunohistochemistry. Under deep anesthesia with isoflurane, mice were transcardially perfused with 3% paraformaldehyde and 1% glutaraldehyde in PBS. The brains and spinal cords were removed and immersed in serially increasing concentrations of a sucrose–PBS solution (final sucrose concentration of 30%). The immunohistochemical procedure was performed on 10-μm-thick sections, which were cut with a cryostat (model HM500 O; Microm). The sections were analyzed with a

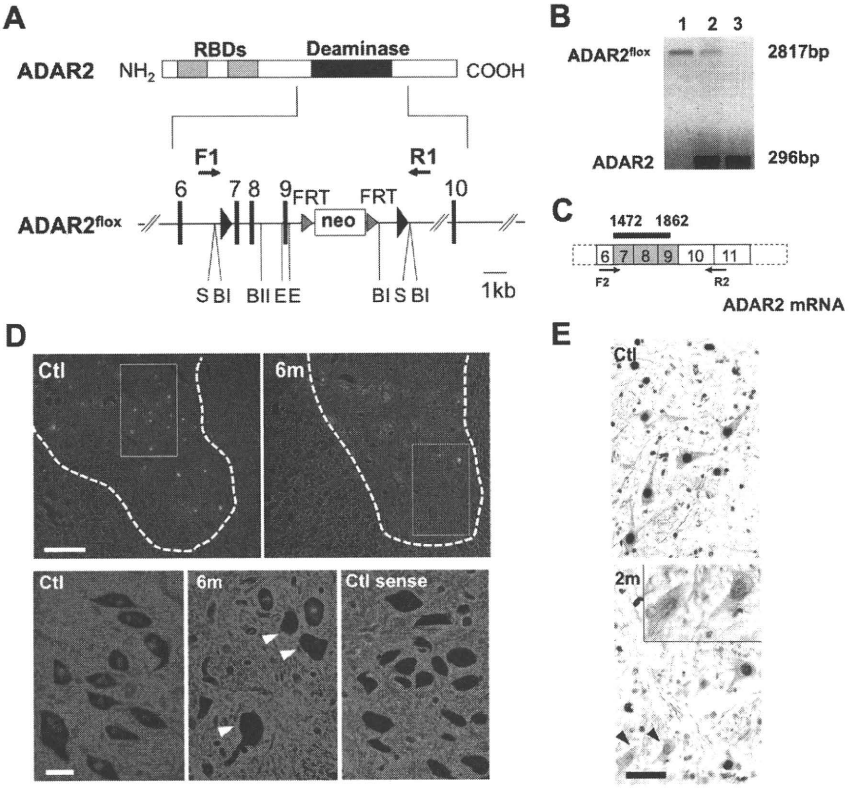

Figure 1. Generation of a conditional ADAR2 knock-out mouse. ***A***, A LoxP site (filled triangle) was inserted into intron 6 and another LoxP site in intron 9 with a selection cassette containing the gene for neomycin resistance (Neo) flanked by FRT sites. Exons are depicted as black bars with numbers. RBDs, RNA binding domains; F1/R1, primer pair (supplemental Table S1, available at www.jneurosci.org as supplemental material) for ***B***; S, SfiI; BI, BglI; BII, BglII; E, ERI. ***B***, Genomic PCR using template DNA obtained from the tails of *ADAR2*$^{flox/flox}$ mice (lane 1), *ADAR2*$^{flox/-}$ mice (lane 2), and *ADAR2*$^{+/+}$ mice (lane 3). ***C***, Exons excised by recombination are shown as shaded areas in the mRNA, and a black bar indicates the *in situ* hybridization probe (supplemental Table S1, available at www.jneurosci.org as supplemental material) for ***D***. F2/R2, Primer pair (supplemental Table S1, available at www.jneurosci.org as supplemental material) used in Figure 2 *B*. ***D***, *In situ* hybridization using a probe that encompasses the region excised by Cre-mediated recombination. There is a large number of punctate signals in the gray matter (outlined with dotted lines) of control mice (Ctl), whereas nuclei of some large neurons in the anterior horn were devoid of signal in the *ADAR2*$^{flox/flox}$/VAChT–Cre.Fast (AR2) mice at 6 months of age (6m; arrowheads in magnified view). The sense probe did not yield a visible signal in the control mice at the same age (Ctl sense). Scale bars: top panels, 200 μm; bottom panels, 25 μm. ***E***, All SMI-32-positive large neurons in the anterior horn (AHCs, brown color in the cytoplasm) of the cervical cord (C5) were ADAR2 positive (dark gray color in the nuclei) in the control mice (Ctl), whereas some of them were devoid of ADAR2 immunoreactivity in AR2 mice at 2 months of age (2m, arrowheads and inset). Sections were counterstained with hematoxylin. Scale bar: 50 μm; inset, 25 μm.

standard avidin–biotin–immunoperoxidase complex method using the M.O.M. Immunodetection kit (Vector Laboratories) for mouse primary antibodies and Vectastain ABC IgGs (Vector Laboratories) for other primary antibodies. The following primary antibodies were used: mouse anti-nonphosphorylated neurofilament H (SMI-32; dilution at 1:1000; Covance), mouse anti-neuronal nuclei (NeuN) (dilution at 1:500; Millipore Bioscience Research Reagents), sheep anti-rat RED1 (ADAR2) N terminus [dilution at 1:500; a gift from Dr. R. B. Emeson (Sansam et al., 2003)], rabbit anti-glial fibrillary acidic protein (GFAP) (dilution at 1:200; Lab Vision), and rat anti-mouse MAC-2 (dilution at 1:500; Cedarlane). Color was developed with the HRP–DAB System (Vector Laboratories).

Muscles and neuromuscular junctions. Medial gastrocnemius muscles and medial quadriceps muscles were dissected, pinned in mild stretch, and mounted on cork blocks and were quickly frozen in isopentane–liquid nitrogen. Samples were stored at −80°C until use. Five-micrometer-thick transverse frozen sections were stained with hematoxylin and eosin. Twenty-micrometer-thick frozen longitudinal sections were stained with tetramethylrhodamine–bungarotoxin. The same section was incubated with monoclonal antibodies to neurofilament (NF160; dilution at 1:200; Millipore Bioscience Research Reagents) and synaptophysin (dilution at 1:100; Cell Signaling Technologies) and then with Alexa Fluor 488 rabbit anti-mouse IgG (dilution at 1:100; Invitrogen) as the secondary antibody. Stained sections were examined under an LSM-510 confocal microscope system (Carl Zeiss).

Electrophysiology. Mice were anesthetized with isoflurane and placed in a prone position on a thermal pad at 37°C for the examination. Electromyogram (EMG) recordings using a Power Lab 26T and EMG machine (AD Instruments) were obtained using a 29-gauge, Teflon-coated, monopolar needle electrode. The recording electrode was inserted into the gastrocnemius muscles, and spontaneous electrical activity was recorded for 120 s using a Lab Chart analysis system (AD Instruments).

Morphological observation and stereology. Sections of the fifth cervical (C5) and fifth lumbar (L5) spinal cord segments were sequentially immunostained with RED1 and SMI-32 using the HRP–DAB system with and without the addition of $NiCl_2$ for color development. Some sections were immunostained with NeuN. ADAR2-positive and -negative neurons were separately counted among SMI-32-positive neurons with diameters larger than 20 μm in 10 sections for each mouse. The number of NeuN-positive neurons with diameter smaller than 20 μm in the ventral gray matter (ventral to the line running though the ventral edge of the central canal) was counted in 10 C5 sections for each mouse at 12 months of age. None of the NeuN-positive small neurons exhibited SMI-32 or GFAP immunoreactivity. The entire brainstem of each mouse at 12 months of age was cut axially to produce a 10-μm-thick section, and the numbers of all the neurons with nucleoli in the nuclei of cranial motor nerves were counted under a light microscope after cresyl violet staining. The position of each nucleus was stereologically determined using a mouse brain atlas (Paxinos and Franklin, 2001). The positions from the bregma were from −3.80 to −4.24 mm (nucleus of oculomotor nerve), from −4.36 to −4.48 mm (nucleus of trochlear nerve), from −4.84 to −5.34 mm (motor nucleus of trigeminal nerve), from −5.52 to −5.80 mm (nucleus of abducens nerve), from −5.68 to −6.48 mm (nucleus of facial nerve), from −7.08 to −7.92 mm (dorsal nucleus of vagus nerve), and from −7.08 to −8.12 mm (nucleus of hypoglossal nerve). The density of neurons in each nucleus was estimated by dividing the total number of neurons in each nucleus by the volume of the nucleus, which was calculated as the product of the area of the nucleus and the thickness of each section. In addition, transverse, 1-μm-thick, Epon-embedded sections of the anterior horns of the spinal cord, and the ventral roots at the L5 level were prepared and stained with 0.1% toluidine blue. Cell counting was performed by researchers who were blind to the genotype of the mouse.

In situ *hybridization.* Anesthetized mice were perfusion fixed with Tissue Fixative (GenoStaff). Dissected cervical cord tissues were sectioned after they were embedded in paraffin. Antisense and sense *adarb1* cRNA probes (Fig. 1*C*) (supplemental Table S1, available at www.jneurosci.org as supplemental material) were generated from the mouse *adarb1* open reading frame sequence, which was cloned into the pGEMT-Easy vector (Promega). Digoxigenin-labeled cRNA probes were prepared with the DIG RNA Labeling mix (Roche Applied Science). Color was developed with nitro blue tetrazolium/5-bromo-4-chloro-3-indolyl phosphate, and tissue sections were counterstained with Kernechtrot stain solution

(Muto Pure Chemicals). After mounting, 24-bit color images were acquired by scanning of the sections. Digoxigenin signals were isolated by uniformly subtracting the counterstaining color component using Photoshop version 9.0.2 (Adobe Systems) (Ohmae et al., 2006; Takemoto-Kimura et al., 2007).

Statistics. Differences in behavior and survival rates between groups were analyzed using log-rank analysis with SPSS software (version 15; SPSS Inc.), and GraphPad Prism version 4 (GraphPad Software), respectively. The differences in neuronal number between each group and the control samples were examined with a repeated-measures ANOVA. The SPSS version 15 software was used for ANOVA, followed by a Tukey–Kramer statistical test.

Results

Generation of the *ADAR2*$^{flox/flox}$/VAChT–Cre mouse, designated as AR2 mouse

We constructed the mouse *ADAR2*^{flox} allele by flanking exons 7–9 of the *adarb1* gene (mouse *ADAR2* gene) with loxP sites (Fig. 1*A*) (supplemental Table S1, available at www.jneurosci.org as supplemental material). Exons 7–9 encode the majority of the adenosine deaminase motif in the *adarb1* gene (Feng et al., 2006), and Cre-mediated deletion of this region ablates ADAR2 activity. To ablate ADAR2 activity selectively in motor neurons, we crossed *ADAR2*$^{flox/flox}$ mice with VAChT–Cre.Fast mice. In VAChT–Cre.Fast mice, Cre expression is under the control of the vesicular acetylcholine transporter gene promoter, which is active in cholinergic neurons, including spinal motor neurons (Misawa et al., 2003). In these transgenic mice, Cre expression is developmentally regulated, and ~50% of motor neurons express Cre by 5 weeks of age, independent of the heterozygous or homozygous state of the transgene (Misawa et al., 2003). The resulting *ADAR2*$^{flox/flox}$/VAChT–Cre.Fast mice, referred to here as AR2 mice (for breeding, see Materials and Methods), therefore would lack ADAR2 activity in a subset of motor neurons in the spinal cord and other brain motor nuclei after expression of Cre by 5 weeks of age. *In situ* hybridization with a probe encompassing the sequence excised by Cre-mediated recombination (Fig. 1*C*) demonstrated that several large neurons in the anterior horn (AHCs) were devoid of *adarb1* gene signal in the AR2 mice, whereas all the AHCs exhibited the signal in control littermates (Fig. 1*D*). Similarly, a subset of the AHCs were devoid of ADAR2 immunoreactivity in AR2 mice, whereas all AHCs exhibited ADAR2 immunoreactivity in the controls (Fig. 1*E*). There was no difference in the results on male and female AR2 mice.

ADAR2 activity in ADAR2-null motor neurons

Next we examined the effects of recombination of the *ADAR2*^{flox} allele on ADAR2 activity. We dissected all large neurons in the anterior horn (AHCs) (for AHC identification, see supplemental Fig. S1*A*, available at www.jneurosci.org as supplemental material) from frozen sections from 2-month-old AR2 mice ($n = 4$) using a laser microdissector (Fig. 2*A*). We verified that these AHCs, but not small neurons in the anterior horn, are the spinal motor neurons by RT-PCR for choline acetyltransferase on a single-cell lysates (supplemental Fig. S1, available at www.jneurosci.org as supplemental material). Because RT-PCR of GluR2 mRNA on the lysates of three neurons, but not the lysates of one or two motor neurons, reproducibly yielded amplification products, we analyzed the extent of GluR2 Q/R site editing on RNA extracted from the lysates of three pooled AHCs (designated as a specimen) by quantitative analysis of the BbvI-restriction digests of the RT-PCR products, as described previously (Kawahara et al., 2003b, 2004). Among 116 specimens examined, eight showed 0% and 42 showed 100% Q/R site editing, with the remaining 66 specimens distributed between the ranges of 17 and 98% (Fig. 2*A*) (supplemental Table S2, available at www.jneurosci.org as supplemental material). Because AHCs of control littermates (these carried wild-type ADAR2 alleles or no Cre transgene; see Materials and Methods) expressed only edited GluR2 mRNA, the presence of samples exhibiting 0% Q/R site editing suggests that ADAR2-expressing neurons expressed only edited GluR2 mRNA, whereas ADAR2-null neurons expressed only unedited GluR2 mRNA. Then, DNA and total RNA from the specimens were collected in four different groups according to the proportions of unedited GluR2 (Fig. 2*A*). Using PCR, we demonstrated that the samples with 100% editing efficiency (group 0:3) harbored the truncated *ADAR2*^{flox} gene and Cre transcripts, whereas the samples with 100% editing efficiency (group 3:0) carried the full-length *ADAR2*^{flox} gene and did not express Cre (Fig. 2*B*). Those samples with both edited and unedited GluR2 mRNA (groups 1:2 and 2:1) exhibited both full-length and truncated ADAR2 along with the Cre transcript. These qualitative results are consistent with the assumption that recombination of the *ADAR2*^{flox} alleles occurred in a Cre-dependent manner and that this recombination abolished the editing of the GluR2 Q/R site. Among other A-to-I sites examined, we found a significant reduction in editing efficiency only at the GluR6 Q/R site (supplemental Table S3, available at www.jneurosci.org as supplemental material).

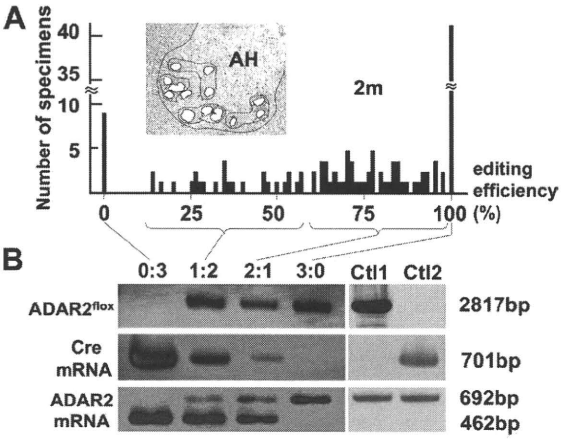

Figure 2. Cre-dependent targeting of ADAR2 and GluR2 Q/R site-editing in motor neurons. ***A***, Frequency histogram of editing efficiency at the GluR2 Q/R site in specimens (lysates containing 3 motor neurons) obtained from AR2 mice at 2 months of age (2m; $n = 4$). Neurons were dissected with a laser microdissector (inset). ***B***, Specimens ($n = 116$) were collected into four groups depending on the predicted number of ADAR2-deficient neurons in each specimen; the groups of specimens containing 3, 2, 1, and 0 unedited GluR2-expressing neurons were designated as groups 0:3, 1:2, 2:1, and 3:0, respectively. The *ADAR2*^{flox} gene and transcripts of the *Cre* gene and the *ADAR2*^{flox} alleles before and after recombination were analyzed for each group by PCR. AHCs expressing unedited GluR2 mRNA (group 0:3) harbored the truncated *ADAR2*^{flox} gene and Cre transcripts, whereas AHCs expressing edited GluR2 mRNA (group 3:0) carried the full-length *ADAR2*^{flox} gene and did not express Cre. Ctl1, *ADAR2*$^{flox/flox}$ mice; Ctl2, VAChT–Cre.Fast mice; AH, anterior horn of the spinal cord.

Behavioral changes

AR2 mice were hypokinetic (supplemental movie, available at www.jneurosci.org as supplemental material) and abnormal in posture (supplemental Fig. S2*A*, available at www.jneurosci.org as supplemental material), but they displayed no overt paralysis or vesico-urinary disturbances and exhibited a normal withdrawal response to noxious stimuli. They showed a lower rotarod performance than their control littermates after 5 weeks of age

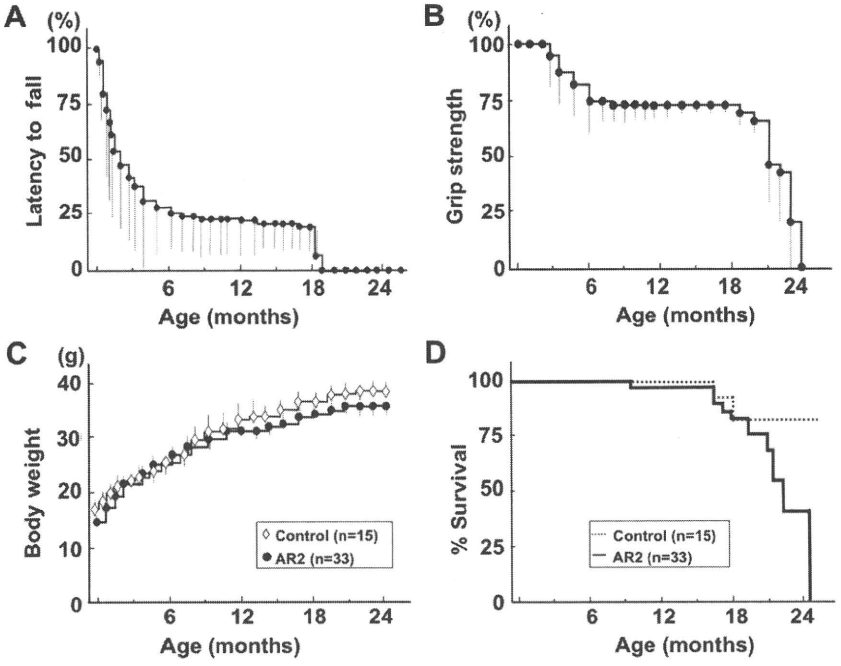

Figure 3. Behavioral changes in AR2 mice. ***A***, Rotarod performance presented as latency to fall (at 10 rpm, 180 s at the maximum) began to decline at 5 weeks of age in AR2 mice and rapidly fell to low levels during the initial 5–6 months, remaining stable until 18 months of age. Control mice exhibited full performance (180 s) until ~12 months of age, followed by slightly lower performance (>164.5 ± 6.4 s) until 24 months. ***B***, Grip strength measured declined with kinetics similar to those of rotarod performance. In ***A*** and ***B***, the scores obtained for the AR2 mice (mean ± SEM; $n = 28$) are indicated as percentage performance of control mice ($n = 15$). ***C***, AR2 mice exhibited slightly lower body weight than controls ($p > 0.05$). ***D***, AR2 mice ($n = 33$) had long lifespans, but the rate of death increased after month 18. The median ± SEM survival was 81.5 ± 16.4 weeks for AR2 mice compared with 105.1 ± 13.5 weeks for control mice ($p = 0.0262$, log-rank analysis).

(Fig. 3*A*), when the Cre expression reached the maximum level (~50% of motor neurons) (Misawa et al., 2003). Their rotarod performance rapidly declined during the initial 5–6 months of life, followed by stable performance until about 18 months of age (Fig. 3*A*). Control mice exhibited full performance (180 s) until ~12 months of age, followed by slightly lower performance (>164.5 ± 6.4 s) until 24 months. Grip strength declined with kinetics similar to those of rotarod performance (Fig. 3*B*). The AR2 mice had slightly lower body weight than the controls (Fig. 3*C*) and were relatively long-lived (81.5 ± 16.4 weeks; mean ± SEM), although not as long as control mice (105.1 ± 13.5 weeks; $p = 0.0262$, log-rank analysis) (Fig. 3*D*).

Pathological alterations in the spinal cords and muscles

Immunohistochemical examination demonstrated that all the AHCs in the spinal cord that were immunoreactive to anti-phosphorylated neurofilament antibodies (SMI-32) showed intense ADAR2 immunoreactivity in their nuclei in control mice, whereas a fraction of these cells was devoid of ADAR2 immunoreactivity in AR2 mice (Fig. 1*E*) (supplemental Fig. S2*B*, available at www.jneurosci.org as supplemental material). There were a number of degenerating AHCs with cytoplasmic vacuoles (Fig. 4*A*) and darkly stained degenerating axons in the ventral roots (Fig. 4*B*). The number of AHCs in AR2 mice markedly decreased between 1 and 2 months of age and then slowly decreased beyond 1 year of age (Fig. 4*C*). The number of ADAR2-positive AHCs in the AR2 mice decreased from 83 to 54% of the number of total AHCs in the age-matched control littermates between 1 and 2 months of age. The rapid reduction in the proportion of ADAR2-positive AHCs during this period is likely attributable to the Cre-dependent recombination of the floxed ADAR2 alleles, because the number of Cre-expressing AHCs in VAChT–Cre-.Fast mice increases developmentally until 5 weeks of age (Misawa et al., 2003). After 2 months of age, the number of ADAR2-positive AHCs did not change over the course of more than 1 year, whereas that of total AHCs decreased from 80 to 54% of the number of AHCs in the age-matched control mice (Fig. 4*C*) (Table 1). Consistent with the Cre-dependent recombination, the proportion of ADAR2-lacking AHCs in AR2 mice is in accordance with that of Cre-expressing AHCs presented in the original study of VAChT–Cre mice (Misawa et al., 2003). Concomitant with AHC degeneration, the number of myelinated axons in the ventral roots was significantly decreased (Table 1).

The kinetics of neuronal loss (Fig. 4*C*) were consistent with the kinetics of progressive motor-selective behavioral deficits (Fig. 3*A*,*B*). The long survival with hypoactivity beyond 6 months of age indicates that the remaining ADAR2-expressing neurons functioned normally during the remainder of life. The high rate of death after 18 months may reflect the failure of the remaining AHCs to compensate for an age-related decline in skeletal muscle power, including a decline in respiratory muscle strength.

We also examined denervation of skeletal muscles. Electromyography performed on AR2 mice at 12 months of age revealed fibrillation potentials and fasciculations, which are common findings in ALS, indicative of muscle fiber denervation and motor unit degeneration and regeneration (Fig. 4*D*). We observed characteristics of denervation, including muscle fiber atrophy, centrally placed nuclei, and pyknotic nuclear clumps in the skeletal muscles of AR2 mice (Fig. 4*E*). Some neuromuscular junctions (NMJs) were not innervated and other NMJs were innervated by ramified axons that innervated more than one NMJ in AR2 mice, indicating reinnervated NMJs (Fig. 4*F*). In contrast, in control mice, all the NMJs were innervated by a single axon. The proportion of denervated NMJs decreased, whereas reinnervated NMJs increased with age in AR2 mice (Fig. 4*F*). In addition, proliferation of activated astrocytes with increased GFAP immunoreactivity and of MAC2-positive activated microglial cells was detected in the anterior horns of AR2 mice (Fig. 4*G*,*H*). These results suggest that degeneration of ADAR2-lacking AHCs induced degeneration of their axon terminals, and then denervated NMJs were reinnervated by collaterally sprouted axons of ADAR2-expressing AHCs after longer survival.

Neurons in the motor nuclei of cranial nerves

The numbers of large neurons in facial and hypoglossal nerve nuclei in AR2 mice were significantly smaller than those in control mice at 12 months of age, whereas the numbers of neurons in nuclei of oculomotor nerves were not decreased (Table 1). Conversely, GluR2 Q/R site editing was significantly decreased both the in oculomotor nerve nuclei (the efficiency of GluR2 Q/R site

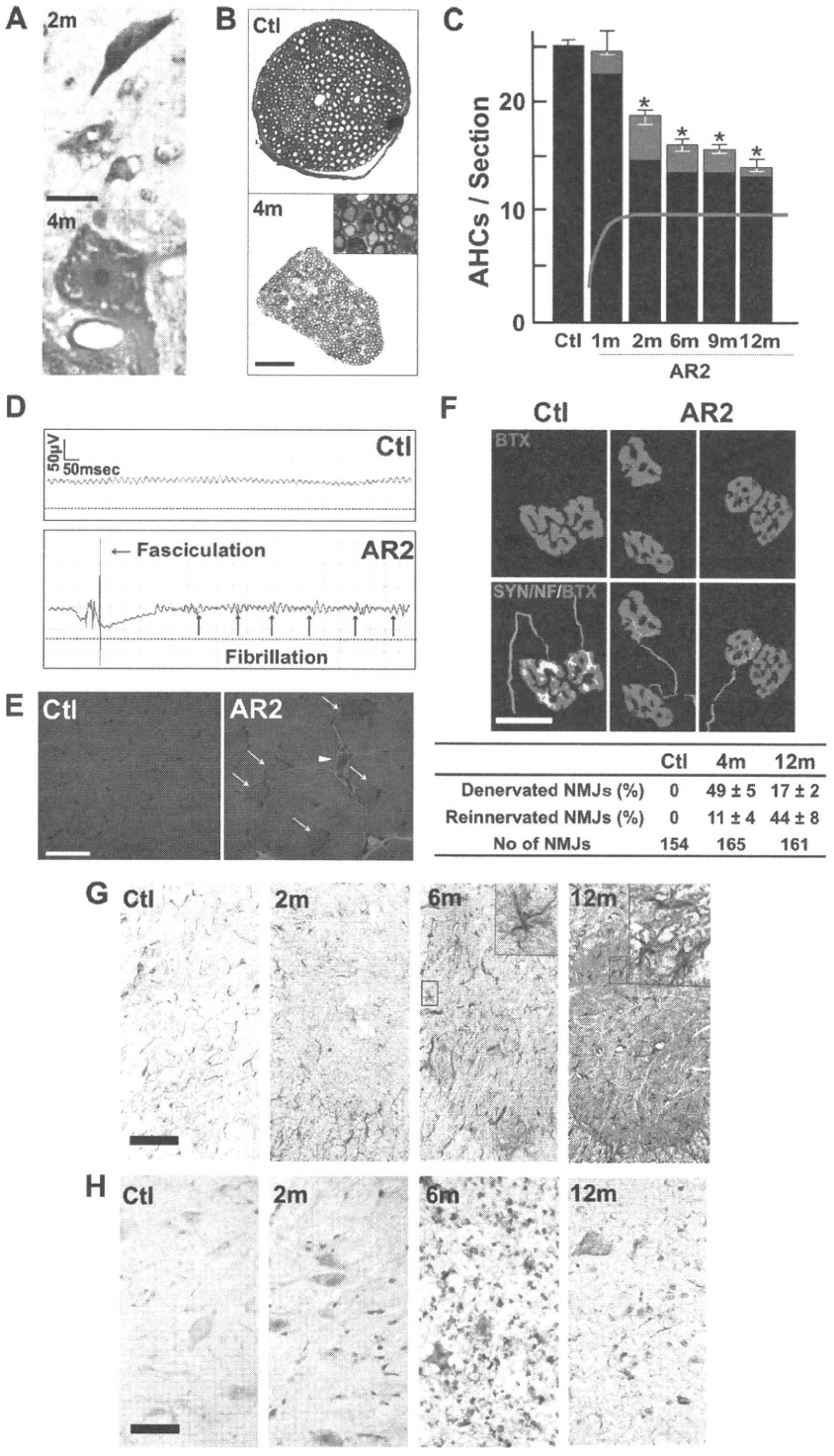

Figure 4. Loss of ADAR2-deficient motor neurons. ***A***, Degenerating AHCs in AR2 mice at 2 months (2m; Nissl staining) and 4 months (4m; toluidine blue staining, 1 μm section) of age. Scale bar: 2m, 25 μm; 4m, 12.5 μm. ***B***, Ventral root (L5) of control (Ctl) and AR2 mice at 4 months of age (4m). Inset, Magnified view of degenerating axons. Scale bar: 100 μm; inset, 20 μm. ***C***, Numbers of AHCs showing ADAR2 immunoreactivity (black columns) and lacking this immunoreactivity (gray columns) (mean ± SEM) in AR2 mice at different ages (1m, 2m, 6m, 9m, 12m). In AR2 mice, Cre expression is developmentally regulated (orange line), and ~50% of motor neurons express Cre by 5 weeks of age, with recombination of the *ADAR2* gene in ~10% of AHCs at 1 month of age and 40–45% of AHCs after 2 months of age (orange line). The number of ADAR2-lacking AHCs significantly decreased in AR2 mice after 2 months of age as a result of Cre-dependent knock-out of ADAR2 (*$p < 0.01$, repeated-measures ANOVA). The number of AHCs in the control mice did not change at different ages, and all the AHCs in controls showed ADAR2 immunoreactivity. ***D***, Electrophysiological examination in AR2 mice. Electromyography from an AR2 mouse at 12 months of age showing fibrillations and fasciculations, common findings in ALS indicative of muscle fiber denervation and motor unit degeneration and regeneration. These findings were observed in two other AR2 mice examined but never in control mice (Ctl; $n = 2$). ***E***, Calf muscles from a wild-type mouse (left) and an AR2 mouse (middle and right) at 12 months of age. Characteristics of denervated muscles, including muscle fiber atrophy (white arrow), centrally placed nuclei, and pyknotic nuclear clumps (white arrowhead) are observed in the AR2 mouse. Hematoxylin and eosin. Scale bar, 60 μm. ***F***, NMJs and distal axons. Quadriceps muscles from a wild-type mouse (Ctl; left) and an AR2 mouse (AR2; middle and right) at 12 months of age are stained with tetramethylrhodamine–bungarotoxin (BTX) (red) and immunostained concomitantly with anti-synaptophysin and neurofilament (SYN/NF) antibodies (green). Endplates (red) were counted as "innervated" if they were merged with axon terminals (merge; yellow). Each endplate is innervated by a thick axon terminal in the Ctl mouse. In AR2 mice, in addition to the normally innervated NMJs, some NMJs were innervated by axons that simultaneously innervate more than one NMJ (reinnervated NMJs; middle), and other NMJs were devoid of axon terminals (denervated NMJs; right). More than 50 NMJs were counted in each animal in the control group and groups of AR2 mice at 4 and 12 months of age ($n = 3$ in each group). Proportions of denervated NMJs and reinnervated NMJs among total NMJs in each group are indicated as mean ± SD (percentage). Scale bar, 25 μm. ***G***, ***H***, Immunohistochemistry in the anterior horn (C5). There was a time-dependent increase in GFAP immunoreactivity (***G***) and an increase in MAC2 immunoreactivity maximal at 6 months of age (***H***) in the spinal anterior horn of AR2 mice. m, Months of age; inset, activated astroglia. Scale bars: ***G***, 100 μm; insets and ***H***, 50 μm.

editing, mean ± SEM: for AR2 mice, 89.7 ± 5.8%, $n = 3$; for control mice, 100%, $n = 3$, $p = 0.0048$) and in the facial nerve nuclei (for AR2 mice, 82.6 ± 9.1%, $n = 3$; for control mice, 99.2 ± 0.2%, $n = 3$, $p = 0.0017$) of AR2 mice at 12 months of age. These results indicate that ADAR2-lacking motor neurons do not always undergo cell death, and some motor neurons, including those in the oculomotor nerve nucleus, are relatively resistant to cell death mediated by deficient ADAR2. Indeed, motor neurons innervating extraocular muscles are much less vulnerable than those innervating bulbar and limb muscles in ALS patients (Lowe and Leigh, 2002).

GluR-B^R alleles prevent motor neuron death in AR2 mice

To investigate by genetic means the role of RNA editing at the GluR2 Q/R site in the death of motor neurons, we exchanged the endogenous *GluR2* alleles in AR2 mice with GluR-B^R alleles (Kask et al., 1998), which directly encode Q/R site-edited GluR2, thus circumventing the requirement for ADAR2-mediated RNA editing. AR2/GluR-$B^{R/R}$ mice were obtained by $ADAR2^{flox/+}$/VAChT–Cre.Fast/GluR-$B^{R/+}$ mice intercrosses to generate $ADAR2^{flox/flox}$/VAChT–Cre.Fast/GluR-$B^{R/R}$ (AR2/GluR-$B^{R/R}$) mice (see Materials and Methods).

Table 1. Density of neurons in motor nerve nuclei and spinal cord

Nucleus	Control ($n = 3$) neurons/mm^3	AR2 ($n = 4$) neurons/mm^3
III	11,253 ± 1783	10,441 ± 632
IV	15,783 ± 1694	16,032 ± 658
VI	10,117 ± 996	10,699 ± 195
Vm	8809 ± 417	8623 ± 246
Vm (>25 μm)	3603 ± 213	2767 ± 175**
VII	1041 ± 124	1016 ± 96
VII (>20 μm)	91.1 ± 32.7	67.7 ± 13.1**
X	11,442 ± 1932	11,652 ± 2387
XII	11,800 ± 541	9834 ± 1530
XII (>20 μm)	832.7 ± 92.9	677.8 ± 116.2**
C5 AH (≤20 μm)	37,147 ± 326	37,941 ± 331
C5 AH (>20 μm)	25.5 ± 0.9[a]	13.7 ± 0.7[a],**
L5 AH (>20 μm)	29.3 ± 0.32[a]	15.9 ± 0.31[a],**
DH	476,312 ± 12,623	498,816 ± 21,446
VR	840.0 ± 26.5[b]	626.3 ± 31.4[b],*

Numbers are the neuronal density per cubic millimeter (mean ± SEM) in each nucleus from mice at 12 months of age. For Vm, VII, and XII, neurons with large diameter (>20 or 25 μm) were also counted. AR2, *ADAR2*$^{flox/flox}$/VAChT–Cre.Fast mice; III, nucleus of oculomotor nerve; IV, nucleus of trochlear nerve; VI, nucleus of abducens nerve; Vm, motor nucleus of trigeminal nerve; VII, nucleus of facial nerve; X, dorsal nucleus of the vagus nerve; XII, nucleus of hypoglossal nerve; C5 AH, anterior horn of the fifth cervical cord; L5 AH, anterior horn of the fifth lumbar cord; DH, zona gelatinosa of the spinal cord; VR, ventral roots (L5). *$p < 0.005$; **$p < 0.001$ (ANOVA).

[a]Number of neurons per section.

[b]Number of axons.

AR2/GluR-$B^{R/R}$ mice (AR2rescue, or AR2res, mice) were phenotypically normal and had full motor function until 6 months of age (Fig. 5*A*). The AHCs, including the ~30% AHCs lacking ADAR2 from Cre-mediated recombination, were viable in AR2res mice at 6 months of age, and the total number of AHCs was the same as in age-matched control mice (Fig. 5*A*,*B*). Consistent with a lack of AHC loss, there was no detectable increase in GFAP or MAC2 immunoreactivity in the anterior horns (supplemental Fig. S2*C*, available at www.jneurosci.org as supplemental material). These results demonstrate that it is specifically the failure of GluR2 Q/R site editing by which ADAR2 deficiency induces the slow death of motor neurons (Fig. 5*C*).

Discussion

We generated the AR2 mouse (Hideyama et al, 2008), a conditional ADAR2 knock-out line, which carries gene-targeted floxed ADAR2 alleles that become functionally ablated by Cre recombinase expressed from a transgene (VAChT–Cre.Fast) in ~50% of motor neurons (Misawa et al., 2003). These displayed progressive motor dysfunctions. The ADAR2-lacking motor neurons expressed only Q/R site-unedited GluR2. Virtually all of the ADAR2-lacking AHCs underwent degeneration, whereas the surviving ADAR2-expressing AHCs remained intact by 12 months of age. The death of ADAR2-lacking AHCs was completely prevented by a point mutation in the endogenous GluR2 alleles of AR2 mice, thus generating Q/R site-edited GluR2 in the absence of ADAR2 (Kask et al., 1998). These findings highlight the crucial role of RNA editing at the GluR2 Q/R site for survival of motor neurons and demonstrate that expression of Q/R site-unedited GluR2 is a cause of slow death of motor neurons. Therefore, it is necessary to investigate the relevance of inefficient GluR2 Q/R site-RNA editing found in the patient's motor neurons to the pathogenesis of sporadic ALS (Kawahara et al., 2004; Kwak and Kawahara, 2005).

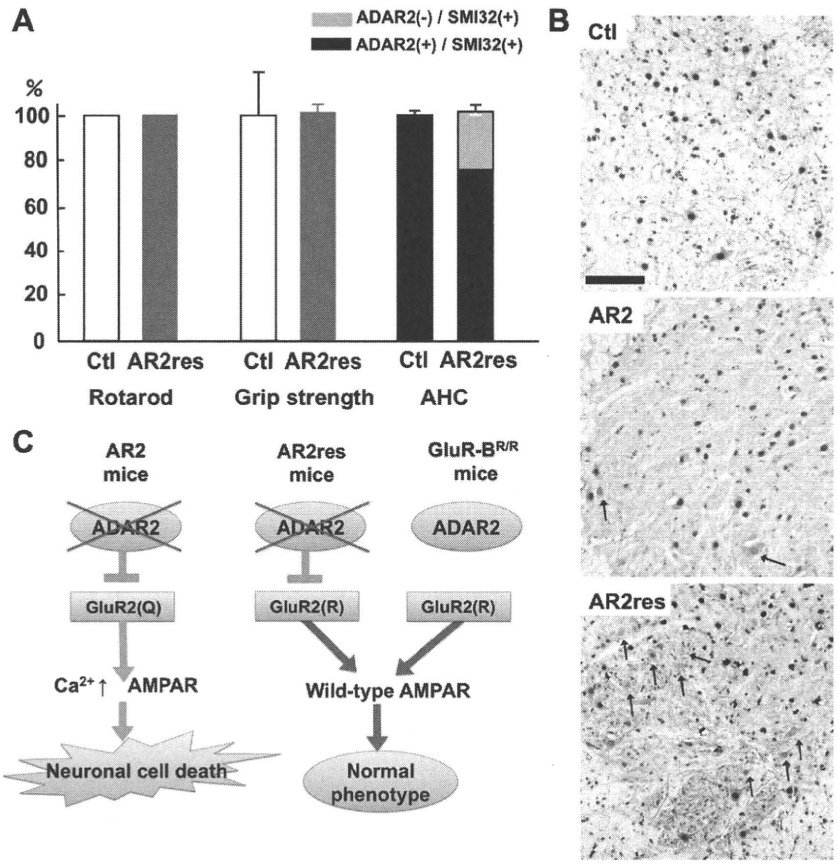

Figure 5. Crucial role of GluR2 Q/R site editing in death of ADAR2-deficient motor neurons. ***A***, AR2/GluR-$B^{R/R}$ mice (AR2res) displayed full rotarod score and normal grip strength at 6 months of age compared with control mice (Ctl). The number of total AHCs, of which a considerable proportion was deficient in ADAR2, did not decrease in AR2res mice. ***B***, At 6 months of age, although only a few AHCs lacking ADAR2 immunoreactivity (arrowheads) were observed in AR2 mice, a considerable number of AHCs lacking ADAR2 immunoreactivity was present in AR2res mice. The density of AHCs in AR2res mice was similar to that in the control mice in which all the AHCs were immunoreactive to ADAR2 in their nuclei. Sections were counterstained with hematoxylin. Scale bar, 100 μm. ***C***, Scheme illustrating that lack of ADAR2 induces slow death of motor neurons in AR2 mice but not in AR2res mice that express Q/R site-edited GluR2 in the absence of ADAR2 activity. The exonic Q codon at the Q/R site of GluR2 was substituted by an R codon in the endogenous GluR2 alleles of GluR-$B^{R/R}$ mice.

Concomitant with the loss of ADAR2-lacking AHCs, proximal and distal axons of AHCs underwent degeneration with resultant neurogenic changes in neuromuscular units. These pathological changes in AHCs and neuromuscular units caused motor dysfunctions in AR2 mice. The prevention of slow neuronal cell death observed in AR2 mice by GluR-B^R alleles expressing Q/R site-edited GluR2 in the absence of ADAR2 (Kask et al., 1998) means that, although ADAR2 edits numerous A-to-I positions in many RNAs expressed in the mammalian brain (Levanon et al., 2004; Li et al., 2009), failure of A-to-I conversions at sites other than the GluR2 Q/R site did not play a role in neuronal cell death (Fig. 5*C*).

When the GluR2 Q/R site is unedited, the Ca^{2+} permeability of the AMPA receptor is greatly increased, and trafficking of the receptor to synaptic membranes is facilitated (Sommer et al., 1991; Burna-

shev et al., 1992; Greger et al., 2002). This enhances neuronal excitability by increasing the density of Ca^{2+}-permeable functional AMPA channels, which is typically observed as fatal epilepsy in mice carrying Q/R site-uneditable GluR-*B* (*GluR2*) alleles (Brusa et al., 1995; Feldmeyer et al., 1999) and in systemic ADAR2-null mice (Higuchi et al., 2000). The results obtained from AR2 mice indicate that motor neurons expressing only Q/R site-unedited GluR2 undergo slow death when the mice live sufficiently long.

Some ADAR2-lacking AHCs die shortly after recombination, whereas others survive for more than 1 year. These observations indicate that, although all the ADAR2-lacking AHCs undergo neuronal death, the ability to compensate for the increased Ca^{2+} overload through the functionally altered AMPA receptor differs among AHCs. It is likely that the increased Ca^{2+} overload might have already led to dysfunction of the ADAR2-lacking AHCs before their death, causing a decline of motor functions at earlier stages. Vulnerability of motor neurons to Ca^{2+}-permeable AMPA receptor-mediated toxicity was demonstrated in GluR-B(N) transgenic mice, which additionally to wild-type GluR2 express an engineered GluR2 subunit that features asparagine (N) in place of glutamine (Q) at the Q/R site (Kuner et al., 2005). ADAR2 activity is downregulated in the rat after transient forebrain ischemia, resulting in the selective death of hippocampal CA1 pyramidal cells (Peng et al., 2006).

An intriguing observation in AR2 mice was the selective vulnerability among motor neurons in different cranial nerve nuclei. Neurons in facial and hypoglossal nerve nuclei decreased in number, whereas those in the oculomotor nerve nuclei did not, although the extent of GluR2 Q/R site editing was significantly reduced in all these nuclei. These results indicate that motor neurons in the oculomotor nerve nuclei can survive despite the incomplete nature of GluR2 Q/R site editing. Notably, motor neurons in the nuclei of oculomotor nerves are also much less vulnerable in ALS patients; this has been attributed to differential expression levels of Ca^{2+}-binding proteins, particularly parvalbumin, among motor neurons in different cranial nerve nuclei. Expression of parvalbumin is high in oculomotor neurons and low in the facial and spinal motor neurons (Ince et al., 1993). Indeed, overexpression of parvalbumin attenuated kainate-induced Ca^{2+} transients and protected spinal motor neurons from resultant neurotoxicity in parvalbumin transgenic mice (Van Den Bosch et al., 2002). It is likely that neurons with an efficient Ca^{2+}-buffering system, such as oculomotor neurons, are resistant to Ca^{2+} overload resulting from Ca^{2+}-permeable AMPA receptors.

The present results indicate that the failure of A-to-I conversion at the Q/R site of GluR2 pre-mRNA in motor neurons of sporadic ALS patients (Takuma et al., 1999; Kawahara et al., 2004; Kwak and Kawahara, 2005) is likely attributable to reduced ADAR2 activity. Indeed, the expression level of ADAR2 mRNA was decreased in the spinal cord of patients with sporadic ALS (Kawahara and Kwak, 2005). Molecular abnormalities found in postmortem tissues of patients with neurodegenerative diseases have shown signs of mechanisms underlying the disease and may represent both the neuronal death process and death-protective reactions arising from the protracted nature of the death process. It is therefore necessary to determine whether these molecular abnormalities are the cause or the result of neuronal cell death by developing an appropriate animal model. Although excitotoxicity has long been implicated in the pathogenesis of neurological diseases including ALS (Vosler et al., 2008; Bezprozvanny, 2009), surprisingly little direct evidence indicating excitotoxic neuronal cell death has been demonstrated in patient-derived materials. Here we demonstrate that the molecular abnormality found in motor neurons of patients with sporadic ALS is a direct cause of neuronal death in mice via a mechanism upregulating Ca^{2+}-permeable AMPA receptors. In addition, the AR2 mice possess certain characteristics found in ALS, including slow progressive death of motor neurons, neuromuscular unit-dependent motor dysfunction and differential low vulnerability of motor neurons of extraocular muscles. Therefore, this mouse model mimicking patient-derived molecular abnormalities may be useful for research on sporadic ALS.

References

Akbarian S, Smith MA, Jones EG (1995) Editing for an AMPA receptor subunit RNA in prefrontal cortex and striatum in Alzheimer's disease, Huntington's disease and schizophrenia. Brain Res 699:297–304.

Beleza-Meireles A, Al-Chalabi A (2009) Genetic studies of amyotrophic lateral sclerosis: controversies and perspectives. Amyotroph Lateral Scler 10:1–14.

Bezprozvanny I (2009) Calcium signaling and neurodegenerative diseases. Trends Mol Med 15:89–100.

Brusa R, Zimmermann F, Koh DS, Feldmeyer D, Gass P, Seeburg PH, Sprengel R (1995) Early-onset epilepsy and postnatal lethality associated with an editing-deficient GluR-B allele in mice. Science 270:1677–1680.

Burnashev N, Monyer H, Seeburg PH, Sakmann B (1992) Divalent ion permeability of AMPA receptor channels is dominated by the edited form of a single subunit. Neuron 8:189–198.

Carriedo SG, Yin HZ, Weiss JH (1996) Motor neurons are selectively vulnerable to AMPA/kainate receptor-mediated injury *in vitro*. J Neurosci 16:4069–4079.

Feldmeyer D, Kask K, Brusa R, Kornau HC, Kolhekar R, Rozov A, Burnashev N, Jensen V, Hvalby O, Sprengel R, Seeburg PH (1999) Neurological dysfunctions in mice expressing different levels of the Q/R site-unedited AMPAR subunit GluR-B. Nat Neurosci 2:57–64.

Feng Y, Sansam CL, Singh M, Emeson RB (2006) Altered RNA editing in mice lacking ADAR2 autoregulation. Mol Cell Biol 26:480–488.

Greger IH, Khatri L, Ziff EB (2002) RNA editing at arg607 controls AMPA receptor exit from the endoplasmic reticulum. Neuron 34:759–772.

Greger IH, Khatri L, Kong X, Ziff EB (2003) AMPA receptor tetramerization is mediated by Q/R editing. Neuron 40:763–774.

Hideyama T, Yamashita T, Tsuji S, Misawa H, Takahashi R, Suzuki T, Kwak S (2008) Slow neuronal death of motor neurons in sporadic ALS mouse model by RNA editing enzyme ADAR2 knockout. Soc Abstr Neurosci 34:745.17.

Higuchi M, Maas S, Single FN, Hartner J, Rozov A, Burnashev N, Feldmeyer D, Sprengel R, Seeburg PH (2000) Point mutation in an AMPA receptor gene rescues lethality in mice deficient in the RNA-editing enzyme ADAR2. Nature 406:78–81.

Ince P, Stout N, Shaw P, Slade J, Hunziker W, Heizmann CW, Baimbridge KG (1993) Parvalbumin and calbindin D-28k in the human motor system and in motor neuron disease. Neuropathol Appl Neurobiol 19:291–299.

Kask K, Zamanillo D, Rozov A, Burnashev N, Sprengel R, Seeburg PH (1998) The AMPA receptor subunit GluR-B in its Q/R site-unedited form is not essential for brain development and function. Proc Natl Acad Sci U S A 95:13777–13782.

Kawahara Y, Kwak S (2005) Excitotoxicity and ALS: what is unique about the AMPA receptors expressed on spinal motor neurons? Amyotroph Lateral Scler Other Motor Neuron Disord 6:131–144.

Kawahara Y, Ito K, Sun H, Kanazawa I, Kwak S (2003a) Low editing efficiency of GluR2 mRNA is associated with a low relative abundance of ADAR2 mRNA in white matter of normal human brain. Eur J Neurosci 18:23–33.

Kawahara Y, Kwak S, Sun H, Ito K, Hashida H, Aizawa H, Jeong SY, Kanazawa I (2003b) Human spinal motoneurons express low relative abundance of GluR2 mRNA: an implication for excitotoxicity in ALS. J Neurochem 85:680–689.

Kawahara Y, Ito K, Sun H, Aizawa H, Kanazawa I, Kwak S (2004) Glutamate receptors: RNA editing and death of motor neurons. Nature 427:801.

Kawahara Y, Sun H, Ito K, Hideyama T, Aoki M, Sobue G, Tsuji S, Kwak S (2006) Underediting of GluR2 mRNA, a neuronal death inducing mo-

lecular change in sporadic ALS, does not occur in motor neurons in ALS1 or SBMA. Neurosci Res 54:11–14.

Kuner R, Groom AJ, Bresink I, Kornau HC, Stefovska V, Müller G, Hartmann B, Tschauner K, Waibel S, Ludolph AC, Ikonomidou C, Seeburg PH, Turski L (2005) Late-onset motoneuron disease caused by a functionally modified AMPA receptor subunit. Proc Natl Acad Sci U S A 102: 5826–5831.

Kwak S, Kawahara Y (2005) Deficient RNA editing of GluR2 and neuronal death in amyotropic lateral sclerosis. J Mol Med 83:110–120.

Levanon EY, Eisenberg E, Yelin R, Nemzer S, Hallegger M, Shemesh R, Fligelman ZY, Shoshan A, Pollock SR, Sztybel D, Olshansky M, Rechavi G, Jantsch MF (2004) Systematic identification of abundant A-to-I editing sites in the human transcriptome. Nat Biotechnol 22:1001–1005.

Li JB, Levanon EY, Yoon JK, Aach J, Xie B, Leproust E, Zhang K, Gao Y, Church GM (2009) Genome-wide identification of human RNA editing sites by parallel DNA capturing and sequencing. Science 324:1210–1213.

Lowe JS, Leigh N (2002) Motor neuron disease (amyotrophic lateral sclerosis). In: The Greenfield's neuropathology (Love S, Louis DN, Ellison DW, eds), pp 372–383. Oxford: Oxford UP.

Melcher T, Maas S, Herb A, Sprengel R, Seeburg PH, Higuchi M (1996) A mammalian RNA editing enzyme. Nature 379:460–464.

Misawa H, Nakata K, Toda K, Matsuura J, Oda Y, Inoue H, Tateno M, Takahashi R (2003) VAChT–Cre.Fast and VAChT–Cre.Slow: postnatal expression of Cre recombinase in somatomotor neurons with different onset. Genesis 37:44–50.

Nishimoto Y, Yamashita T, Hideyama T, Tsuji S, Suzuki N, Kwak S (2008) Determination of editors at the novel A-to-I editing positions. Neurosci Res 61:201–206.

Ohmae S, Takemoto-Kimura S, Okamura M, Adachi-Morishima A, Nonaka M, Fuse T, Kida S, Tanji M, Furuyashiki T, Arakawa Y, Narumiya S, Okuno H, Bito H (2006) Molecular identification and characterization of a family of kinases with homology to Ca^{2+}/calmodulin-dependent protein kinases I/IV. J Biol Chem 281:20427–20439.

Paschen W, Hedreen JC, Ross CA (1994) RNA editing of the glutamate receptor subunits GluR2 and GluR6 in human brain tissue. J Neurochem 63:1596–1602.

Paxinos G, Franklin KBJ (2001) The mouse brain in stereotaxic coordinates. San Diego: Academic.

Peng PL, Zhong X, Tu W, Soundarapandian MM, Molner P, Zhu D, Lau L, Liu S, Liu F, Lu Y (2006) ADAR2-dependent RNA editing of AMPA receptor subunit GluR2 determines vulnerability of neurons in forebrain ischemia. Neuron 49:719–733.

Rothstein JD, Martin LJ, Kuncl RW (1992) Decreased glutamate transporter by the brain and spinal cord in amyotrophic lateral sclerosis. N Engl J Med 326:1464–1468.

Sansam CL, Wells KS, Emeson RB (2003) Modulation of RNA editing by functional nucleolar sequestration of ADAR2. Proc Natl Acad Sci U S A 100:14018–14023.

Schymick JC, Talbot K, Traynor BJ (2007) Genetics of sporadic amyotrophic lateral sclerosis. Hum Mol Genet 16 [Spec No 2]:R233–R242.

Seeburg PH (2002) A-to-I editing: new and old sites, functions and speculations. Neuron 35:17–20.

Sommer B, Köhler M, Sprengel R, Seeburg PH (1991) RNA editing in brain controls a determinant of ion flow in glutamate-gated channels. Cell 67:11–19.

Suzuki T, Tsuzuki K, Kameyama K, Kwak S (2003) Recent advances in the study of AMPA receptors. Nippon Yakurigaku Zasshi 122:515–526.

Takemoto-Kimura S, Ageta-Ishihara N, Nonaka M, Adachi-Morishima A, Mano T, Okamura M, Fujii H, Fuse T, Hoshino M, Suzuki S, Kojima M, Mishina M, Okuno H, Bito H (2007) Regulation of dendritogenesis via a lipid-raft-associated Ca^{2+}/calmodulin-dependent protein kinase CLICK-III/CaMKIgamma. Neuron 54:755–770.

Takuma H, Kwak S, Yoshizawa T, Kanazawa I (1999) Reduction of GluR2 RNA editing, a molecular change that increases calcium influx through AMPA receptors, selective in the spinal ventral gray of patients with amyotrophic lateral sclerosis. Ann Neurol 46:806–815.

Van Damme P, Braeken D, Callewaert G, Robberecht W, Van Den Bosch L (2005) GluR2 deficiency accelerates motor neuron degeneration in a mouse model of amyotrophic lateral sclerosis. J Neuropathol Exp Neurol 64:605–612.

Van Den Bosch L, Schwaller B, Vleminckx V, Meijers B, Stork S, Ruehlicke T, Van Houtte E, Klaassen H, Celio MR, Missiaen L, Robberecht W, Berchtold MW (2002) Protective effect of parvalbumin on excitotoxic motor neuron death. Exp Neurol 174:150–161.

Vosler PS, Brennan CS, Chen J (2008) Calpain-mediated signaling mechanisms in neuronal injury and neurodegeneration. Mol Neurobiol 38: 78–100.

Yang JH, Sklar P, Axel R, Maniatis T (1995) Editing of glutamate receptor subunit B pre-mRNA in vitro by site-specific deamination of adenosine. Nature 374:77–81.

疾患特異的 iPS 細胞を用いた神経変性疾患の研究

八幡　直樹，井上　治久

日本生物学的精神医学会誌　21 巻 4 号別刷

特集2　認知症最前線

2．疾患特異的iPS細胞を用いた神経変性疾患の研究

八幡　直樹[1,2]，井上　治久[1,2]

抄録：数種類の初期化遺伝子を体細胞に導入することにより，胚性幹細胞（embryonic stem cells：ES細胞）に匹敵する多分化能を有する人工多能性幹細胞（induced pluripotent stem cells：iPS細胞）が誕生した。神経変性疾患研究においては，これまで生体から入手が困難であった疾患の標的細胞をiPS細胞から作製することが可能になり，病態解明，創薬開発が進展すると期待されている。本稿では疾患特異的iPS細胞を用いた神経変性疾患研究と今後の展望について述べる。

日本生物学的精神医学会誌 21（4）：257−260, 2010

Key words：iPS cell, Neurodegenerative disease, drug discovery, disease modelling

1．はじめに

2006年，マウス線維芽細胞にレトロウイルスを用いて4つの初期化遺伝子（Oct3/4，Sox2，Klf4，c−Myc）を導入することによりES細胞に匹敵する多分化能を有する細胞を樹立できることが報告された[16]。この細胞は，人工多能性幹細胞（iPS細胞）と命名された。2007年，ヒトにおいても同様に，線維芽細胞からiPS細胞が樹立された[17]。iPS細胞作製技術によって，体細胞を初期化することにより疾患を有する患者さん自身の体細胞から，疾患特異的iPS細胞を経て，疾患の標的細胞を作り出すことが可能になった。特に，ES細胞の倫理的課題や拒絶反応を回避できるため，再生医療の分野にさらなる進展をもたらす可能性がある。神経変性疾患においては，生検により標的細胞を採取することは難しく，また，剖検組織は死後変化等の影響を排除しにくい。神経変性疾特異的iPS細胞を分化誘導することで，疾患標的細胞が作製可能になる。

近年，いくつかの神経変性疾患では，神経細胞自体が抱える要因だけではなく，周囲に存在するグリア細胞が神経変性に関与していることが明らかになっている[2,18]。iPS細胞作製技術を用いることで，神経細胞以外の細胞にも焦点を当てた複合的なアプローチが展開できる可能性がある。本稿では，神経変性疾患におけるiPS細胞研究の現状を概説し，病態解明，創薬開発へ向けての今後の展望を述べる。

2．神経変性疾患特異的iPS細胞研究の現状

2008年，ハーバード大学のグループらが，筋萎縮性側索硬化症（Amyotrophic lateral screlosis; ALS）の原因遺伝子の一つであるsuperoxide dismutase 1（SOD1）の変異を有する患者の皮膚線維芽細胞を用いて，iPS細胞を樹立し，motor neuron and pancreas homeobox 1（HB9）を発現する脊髄運動神経へ分化誘導を行った[4]。同年，パーキンソン病等，多種の疾患特異的iPS細胞作製の報告がある[11]。2009年に，MITのグループらが，初期化遺伝子のゲノムへの挿入がない，パーキンソン病由来iPS細胞を作製し，これらのiPS細胞をtyrosine hydroxylase（TH）陽性ドーパミン作動性神経細胞へ分化誘導を行った[10]。

2009年，survival of motor neuron 1（SMN1）遺伝子の異常による脊髄性筋萎縮症（Spinal muscular atrophy：SMA）について，疾患特異的iPS細胞を利用し，病態再現が示された[5]。SMA患者のiPS細胞を脊髄運動神経に分化誘導すると，6週間後に数および大きさの低下がみられた。また，

Neurodegenerative disease-specific induced pluripotent stem cell research

1）京都大学 iPS細胞研究所臨床応用研究部門（〒606−8507 京都市左京区聖護院川原町53）Naoki Yahata, Haruhisa Inoue：Center for iPS Cell Research and Application（CiRA）, Department of Clinical application, Kyoto University, 53 Kawahara-cho, Shogoin, Sakyo-ku, Kyoto 606-8507, Japan.

2）戦略的創造研究推進事業（CREST），独立行政法人科学技術振興機構（JST）（〒332−0012 埼玉県川口市本町4−1−8）CREST, JST, 4-1-8 Honcho, Kawaguchi, Saitama 332-0012, Japan.

【井上　治久　E-mail：haruhisa@cirakyoto-u.ac.jp】

SMA患者で発現が低下しているSMNの発現を上昇させる薬剤としてしられる，バルプロ酸やトブラマイシンを投与することにより，SMNの発現が上昇し，正常レベルに近づくことが示された。同年，家族性自律神経失調症（Familial dysautonomia：FD）患者由来iPS細胞を用いた病態再現の報告がなされた[7]。この疾患は末梢神経障害を呈し，IKB kinase complex-associated protein（IKBKAP）遺伝子変異によって引き起こされる。FD患者由来iPS細胞から分化した細胞においてIKBKAPのスプライス異常産物の上昇がみられた。また，FD患者由来iPS細胞を神経堤細胞に分化誘導したところ，achaete-scute complex homolog 1（ASCL1）およびβ-III-tubulin（Tuj1）陽性の末梢神経の数の低下や，スクラッチアッセイという方法での細胞移動の異常が観察された。さらに，IKBKAPのスプライス異常産物を減少させるとして知られるカイネチンをiPS細胞培養時に4週間処理することにより，スプライシング異常が改善した。これらの報告は，疾患特異的iPS細胞から分化誘導した細胞を使って，病態再現が可能であることと，分子生物学・生化学的解析により評価可能であることを示している。さらには，疾患特異的iPS細胞が創薬開発のためのスクリーニングに利用可能であることを示している。

3．神経変性疾患特異的iPS細胞を用いた創薬開発

ヒトで効果のある神経変性疾患治療の薬剤を開発するために，ヒトのiPS細胞から分化誘導した標的細胞が薬剤のスクリーニングに使用可能である。このスクリーニング系を構築する際に，標的となる神経細胞やグリア細胞を純度高く，大量に準備することが重要である。これを実現するためには，目的の細胞を効率よく分化誘導する技術に加え，その細胞を純化する技術が必要になる。方法としては，目的の細胞で特異的に発現する遺伝子のプロモーター制御下に蛍光タンパク質を発現するベクターを導入した細胞，あるいは目的細胞特異的な表面抗原を認識する抗体で標識をした細胞をフローサイトメトリーで回収する方法等が行われている[12]。細胞純化技術は細胞移植を行う際にも必須になると考える。疾患特異的iPS細胞を用いた創薬開発への応用には，さらに効率のよい分化誘導・純化法が重要になるであろう。

4．今後の展望

神経系への分化誘導法は，マウスES細胞の系で確立された方法を基礎に，ヒトES細胞を用いて改変がなされている。脊髄運動神経や，ドーパミン作動性神経の分化誘導法は既にいくつかのグループから報告があり[6,15]，上述の運動神経疾患やパーキンソン病の研究に用いられている。しかし，現在まで確立されている脊髄運動神経，ドーパミン作動性神経を含むさまざまな神経への分化誘導法は分化効率や時間などの観点からさらなる効率化の余地がある。ヒトES/iPS細胞からの神経堤細胞[8]，網膜細胞[10]等への分化誘導法についても既に報告がある。最近，マウスのES細胞より小脳プルキンエ細胞への効率的な分化誘導法について報告がなされ，脊髄小脳変性症の病態解明や治療法開発に向けて，ヒトiPS細胞からの誘導法への応用が期待されている[9]。

これまでiPS細胞作製技術を利用して疾患再現が行われた疾患[1,3,5,7,13]は，ほとんどが発生過程の異常がその病態に反映される疾患である。一方で，アルツハイマー病やパーキンソン病などの晩発性神経変性疾患の場合，加齢が危険因子の一つであり，発生過程における異常の有無は不明である。さらに，神経細胞に分化誘導し，成熟化した後に初めて何らかの異常や，疾患由来でない細胞との違いが観察される可能性がある。加齢変化を*in vitro*で再現するために長期の培養や，さらには加齢を加速する培養条件の検討が必要かもしれない。

神経変性疾患において原因遺伝子が同定されたものは，動物モデルや細胞モデルを用いて病態解明が進んでいる。一方，孤発性神経変性疾患の多くは，その病因が依然として不明である。iPS細胞作製技術を用いて，孤発性疾患についても患者由来の標的細胞が手に入ることから，病態解明に新たなアプローチが加わったと考えられる。孤発性神経変性疾患由来iPS細胞から分化誘導した神経細胞について，生化学的・細胞生物学的異常を解析することができれば，創薬開発の分子標的の発見につながるかもしれない。一方，家族性神経変性疾患由来iPS細胞を用いた病態再現を基準に，同じ系で孤発性神経変性疾患由来iPS細胞を用いて病態が再現できれば，診断法開発に寄与する可能性がある。

5．おわりに

本稿では，iPS細胞を用いた神経変性疾患研究について述べた。iPS細胞技術という革新的技術を用

いることによって，神経変性疾患の病態解明および創薬開発が加速することが期待される。

6．謝　辞

認知症の共同研究者である筑波大学の朝田隆先生，長崎大学の岩田修永先生，理化学研究所の西道隆臣先生，放射線医学総合研究所の須原哲也先生，樋口真人先生，神戸大学の戸田達史先生，小林千浩先生，徳島大学の和泉唯信先生，山形大学の川勝忍先生に深謝申し上げます。

文　献

1）Agarwal S, Loh YH, McLoughlin EM, et al (2010) Telomere elongation in induced pluripotent stem cells from dyskeratosis congenita patients. Nature. 464 (7286) : 292-296.
2）Boillée S, Yamanaka K, Lobsiger CS, et al (2006) Onset and progression in inherited ALS determined by motor neurons and microglia. Science. 312 (5778) : 1389-1392.
3）Carvajal-Vergara X, Sevilla A, et al (2010) Patient-specific induced pluripotent stem-cell-derived models of LEOPARD syndrome. Nature. 465 (7299) : 808-812.
4）Dimos JT, Rodolfa KT, Niakan KK, et al (2008) Induced pluripotent stem cells generated from patients with ALS can be differentiated into motor neurons. Science. 321 (5893) : 1218-1221.
5）Ebert AD, Yu J, Rose FF Jr, et al (2009) Induced pluripotent stem cells from a spinal muscular atrophy patient. Nature. 457 (7227) : 277-280.
6）Hu BY and Zhang SC (2009) Differentiation of spinal motor neurons from pluripotent human stem cells. Nat Protoc. 4 (9) : 1295-1304.
7）Lee G, Papapetrou EP, Kim H, et al (2009) Modelling pathogenesis and treatment of familial dysautonomia using patient-specific iPSCs. Nature. 461 (7262) : 402-406.
8）Lee G, Chambers SM, Tomishima MJ, et al (2010) Derivation of neural crest cells from human pluripotent stem cells. Nat Protoc. 5 (4) : 688-701.
9）Muguruma K, Nishiyama A, Ono Y, et al (2010) Ontogeny-recapitulating generation and tissue integration of ES cell-derived Purkinje cells. Nat Neurosci. 13 (10) : 1171-1180.
10）Osakada F, Jin ZB, Hirami Y, et al (2009) In vitro differentiation of retinal cells from human pluripotent stem cells by small-molecule induction. J Cell Sci. 122 (Pt 17) : 3169-3179.
11）Park IH, Arora N, Huo H, et al (2008) Disease-specific induced pluripotent stem cells. Cell. 134 (5) : 877-886.
12）Pruszak J, Sonntag KC, Aung MH, et al (2007) Markers and methods for cell sorting of human embryonic stem cell-derived neural cell populations. Stem Cells. 25 (9) : 2257-2268.
13）Raya A, Rodríguez-Pizà I, Guenechea G, et al (2009) Disease-corrected haematopoietic progenitors from Fanconi anaemia induced pluripotent stem cells. Nature. 460 (7251) : 53-59.
14）Soldner F, Hockemeyer D, Beard C, et al (2009) Parkinson's disease patient-derived induced pluripotent stem cells free of viral reprogramming factors. Cell. 136 (5) : 964-977.
15）Sonntag KC, Pruszak J, Yoshizaki T, et al (2007) Enhanced yield of neuroepithelial precursors and midbrain-like dopaminergic neurons from human embryonic stem cells using the bone morphogenic protein antagonist noggin. Stem Cells. 25 (2) : 411-418.
16）Takahashi K and Yamanaka S (2006) Induction of pluripotent stem cells from mouse embryonic and adult fibroblast cultures by defined factors. Cell. 126 (4) : 663-676.
17）Takahashi K, Tanabe K, Ohnuki M, et al (2007) Induction of pluripotent stem cells from adult human fibroblasts by defined factors. Cell. 131 (5) : 861-872.
18）Yamanaka K, Chun SJ, Boillee S, et al (2008) Astrocytes as determinants of disease progression in inherited amyotrophic lateral sclerosis. Nat Neurosci. 11 (3) : 251-253.

■ ABSTRACT

Neurodegenerative disease-specific induced pluripotent stem cell research

Naoki Yahata, Haruhisa Inoue

Center for iPS Cell Research and Application, Kyoto University

Induced pluripotent stem (iPS) cell technology shows great potential for the study of pathogenesis, and drug discovery toward neurodegenerative diseases. This review summarizes the current status on the neurodegenerative disease-specific iPS cell research and describes its potential.

(Japanese Journal of Biological Psychiatry 21 (4) : 257-260, 2010)

EXPERIMENTAL CELL RESEARCH 316 (2010) 2560–2564

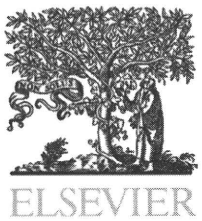

available at www.sciencedirect.com

ScienceDirect

www.elsevier.com/locate/yexcr

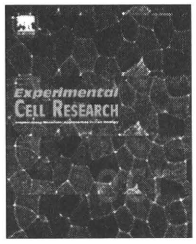

Review

Neurodegenerative disease-specific induced pluripotent stem cell research

*Haruhisa Inoue**

Center for iPS Cell Research and Application, Kyoto University, 53, Kawahara-cho, Shogoin, Sakyo-ku, Kyoto 606-8507, Japan
Japan Science and Technology Agency, CREST, Kawaguchi, Japan

ARTICLE INFORMATION

Article Chronology:
Received 6 April 2010
Accepted 19 April 2010
Available online 24 April 2010

Keywords:
Neurodegenerative disease
Non-neuronal cells
Disease modeling
Disease material
Disease therapy

ABSTRACT

Neurodegenerative disease-specific induced pluripotent stem cell (iPSC) research contributes to the following 3 areas; "Disease modeling", "Disease material" and "Disease therapy".
"Disease modeling", by recapitulating the disease phenotype *in vitro*, will reveal the pathomechanisms. Neurodegenerative disease-specific iPSC-derived non-neuronal cells harboring disease-causative protein(s), which play critical roles in neurodegeneration including motor neuron degeneration in amyotrophic lateral sclerosis, could be "Disease material", the target cell(s) for drug screening. These differentiated cells also could be used for "Disease therapy", an autologous cellular replacement/neuroprotection strategy, for patients with neurodegenerative disease.
Further progress in these areas of research can be made for currently incurable neurodegenerative diseases.

Contents

Neurodegenerative diseases are caused by the degeneration of selected neurons: cortical neurons in Alzheimers' disease, dementia with Lewy bodies, or frontotemporal lobar degeneration, midbrain dopaminergic neurons in Parkinson's disease, cerebellar neurons in spinocerebellar degeneration, and upper and lower motor neurons in amyotrophic lateral sclerosis (ALS). It is widely believed that neurodegenerative diseases generally arise through the same process; neuronal dysfunction [1], the gradual accumulation of misfolded protein and the acceleration of aggregate formation [2], neuronal death [3], and disease progression caused by non-neuronal cells [4,5].

* Fax: +81 75 366 7094.
E-mail address: haruhisa@cira.kyoto-u.ac.jp.

0014-4827/$ – see front matter © 2010 Elsevier Inc. All rights reserved.
doi:10.1016/j.yexcr.2010.04.022